

Christos Christodoulou
Department of Electrical and
Computer Engineering
University of New Mexico
Albuquerque, NM 87131-1356 USA
Tel: +1 (505) 277 6580
Fax: +1 (505) 277 1439
E-mail: christos@ece.unm.edu



Eva Rajo-Iglesias
Departamento de Teoría de la
Señal y Comunicaciones
University Carlos III of Madrid,
Despacho 4.3B10
Avenida de la Universidad,
30, 28911 Leganés, Madrid, Spain
Tel: +34 91 624 8774
Fax: +34 91 624 8749
E-mail: eva@tsc.uc3m.es

Room-Coverage Improvements in UHF RFID with Commodity Hardware

Antonis G. Dimitriou¹, Aggelos Bletsas², and John N. Sahalos³

¹Department of Electrical & Computer Engineering, Aristotle University of Thessaloniki
AUTH Campus, ECE Dept., Egnatia Street, 54124, Thessaloniki, Greece
Tel: +302310994370; E-mail: antodimi@auth.gr

²Department of Electronic & Computer Engineering, Technical University of Crete
TUC Campus, Kounoupidiana, 73100, Chania, Greece
Tel: +302821037377; E-mail: aggelos@telecom.tuc.gr

³Department of Electrical & Computer Engineering, University of Nicosia
Makedonitissas Ave. 46, 1700, Nicosia, Cyprus
Tel: +35722841740; E-mail: sahalos.j@unic.ac.cy

Abstract

This work studies the three-dimensional (3D) identification performance of UHF RFID systems with commodity hardware. Detailed three-dimensional propagation modeling is developed, with ray-tracing that allows examination of tag- as well as reader-antenna diversity. It is shown that multipath can enhance identification performance compared to free-space conditions. Furthermore, it is found that tag diversity can enhance identification performance on the order of 10%. Reader-antenna diversity becomes beneficial only when special attention is given to controlling the destructive summation of the transmitted fields and simple, general antenna-installation rules are provided. Performance can be further enhanced with the introduction of a phase shifter or appropriate transmission scheduling, and various examples are discussed. Measurements inside a room with a dense three-dimensional grid of passive RFID tags confirmed the results. Finally, a method to perform power-measurements with commodity RFID hardware that exploits the sensitivity-during-read threshold of each tag is put forth.

Keywords: Radiofrequency identification; RFID tags; UHF propagation; multipath channels; ray tracing; electromagnetic measurements

1. Introduction

Radio-Frequency Identification (RFID) has been widely adopted in several applications, including asset management, product tracking, logistics, inventory systems, security, location-based services, and many more [1]. UHF RFID systems have extended the identification range of the original LF or HF RFID systems. Depending on the type of tags implemented, a UHF EPC Gen2 operating RFID reader can identify passive tags within a few meters, or active tags within tens of meters. Elementary ideas on backscatter-radio related to RFID systems were given in [2].

In order to acquire accurate read-region estimations, the site-specific nature of propagation must be accounted for. Propagation was analyzed stochastically in [3], where multipath was modeled by a suitable Ricean or Rayleigh distribution. Hence, the probability for successful identification of a tag could be evaluated. A stochastic model, suitable for multiple reader and tag antennas, was presented in [4], where diversity gains were investigated by utilizing multiple tags.

Recently, in [5], the authors proposed a model suitable for single-lobe directional antennas that evaluates the “reliable” reading region in the presence of multipath. They estimated a continuous and strictly bounded “useful reading region” around the transmitting reader’s antenna in a fashion similar to that in which the free-space-model’s reading region is bounded and continuous. To achieve that, they approximated the minimum resulting field of a two-ray model, composed of the direct ray and a ray reflected from the closest wall in the direction of reader antenna’s maximum gain. The read-region was approximated by an ellipsoid, including the reader antenna’s location, while its axes depended on the half-power beamwidth of the antenna. The validity of the proposed model in [5], depends on the location and the direction of the reader’s antenna with respect to the surrounding walls: the basic assumption is that the direct field interacts with a single reflector. Good agreement with measurements was demonstrated for representative configurations. However, the model fails if two or more antennas are fed via a splitter, as the resulting field, due to the interaction of the two antennas, is complex and the corresponding coverage region is not continuous, even in the vicinity of the antennas, as demonstrated later in this work.

In this paper, we investigate the problem of maximizing the coverage of a UHF RFID system operating inside a single room with commodity RFID hardware. This represents part of a greater study that includes the design and implementation of a pilot RFID system inside a hospital [6]. Passive tags are attached to medical equipment, such as infusion pumps and wheelchairs. The main goal is to maximize the identification percentage within a given volume of interest. In Figure 1, a room with the volume of interest is shown.

In contrast to [5], we do not seek a continuous bounded volume where 100% coverage can be guaranteed. Instead, we try to analyze major propagation effects taking place inside a room, and to manipulate them, either to maximize the read-region in the entire volume of interest, or to introduce minima at selected locations inside the room. Certain rules, applicable to any room, regarding the selection of antenna(s) and their placement and orientation are proposed. Furthermore, the tags’ polarization diversity is investigated, and such performance gains are quantified. It is shown that the successful-identification volume in a room, considering multipath, can be larger than the corresponding successful-identification volume in free space. Finally, we propose and evaluate two methods to improve coverage performance through the

utilization of double-reader-antenna systems. The first method is based on selective introduction of a controlled phase shifter in a double-reader-antenna configuration. That method is capable of minimizing destructive-interference patterns, and thus boosts identification performance and reliability of the system. The second method utilizes simple time-scheduling of the operation of each reader’s antenna.

The core of our work is an analytic ray-tracing propagation model. Critical parameters of the problem are carefully modeled, including the radiation pattern, the transmission power, the polarizations of the readers’ antennas as well as of the tags’ antennas, the frequency of operation, the constitutive parameters of the walls, and polarization changes of the reflected field with respect to the incident field.

All theoretical results were verified by extensive measurements carried out in a room, where a three-dimensional grid, composed of orthogonally polarized passive tags, was realized. A method to use passive tags so as to carry out propagation measurements is presented. Preliminary results of this work were presented in [7, 8], including the propagation model.

The propagation model is introduced in Section 2, and “successful identification” is discussed in Section 3. Theoretical results for single-antenna configurations are given in Section 4. These are then compared with double-antenna configurations in Section 5. Methods for improvement of coverage performance with double-antenna configurations are given in Section 6, and the corresponding measurements are presented in Section 7. Finally, a discussion in Section 8 concludes the paper.

2. Propagation Model

Ray-tracing is a common technique for acquiring detailed site-specific propagation data in multipath environments [9]. A ray-tracing model [10], including the direct and the multiple reflected fields at each location, was developed. The operating fre-

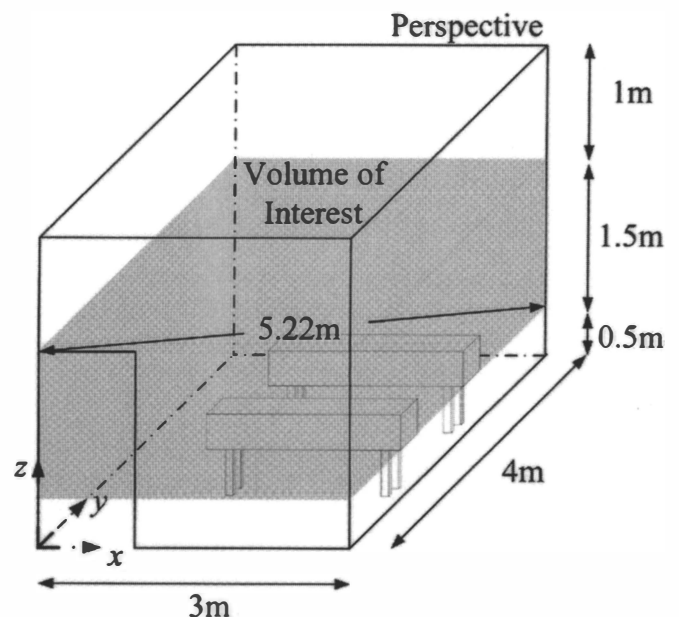


Figure 1. A representation of the room, including the volume of interest.

quency, the transmission power, the radiation pattern, the polarization, the position, and the orientation of the transmitting antenna were included in the calculation of the incident field. Proper algorithms for the manipulation of vectors and their transformations among different spherical and Cartesian coordinate systems have been realized [11].

For a linearly polarized antenna, the magnitude of the radiated-wave electric far-field component, E_{inc} , at a distance r is given by

$$E_{inc} = \sqrt{\frac{\eta P_t G_t(\theta, \phi)}{2\pi}} \frac{1}{r}. \quad (1)$$

P_t is the transmitted power in watts, $G_t(\theta, \phi)$ is the antenna's gain at angles θ, ϕ , and η is the free-space impedance. In order to model a circularly polarized antenna, another field vector, orthogonal to the above, is considered, with a $\pi/2$ phase difference.

For each reflection, the incident field on the boundaries of a wall are analyzed in two orthogonal vectors: one parallel to the plane of incidence, and one perpendicular to the plane of incidence. The reflection coefficients are then calculated by employing the recursive formulation presented in [12, Chapter 5.5.2.D, pp. 235-236]: a plane wave incident at an oblique angle upon N layers of planar dielectric slabs that are bordered on either side by free space is considered. The constitutive parameters of the wall are taken into account by selecting the permittivity and the loss tangent of each layer [13-16]. Each reflection might lead to a different phase shift and magnitude change of the vertically and the horizontally polarized components of the incident field, respectively, thus leading to a change in the polarization state of the reflected field with respect to that of the incident field.

The reflected field is considered to be the incident field in the subsequent interaction with a wall. Finally, the ray is traced until it reaches the receiving position. At the receiver, the field from each path is decomposed into three orthogonally arranged axes, x, y, z . Assuming that the electric field's component of the i th ray along the tag's polarization axis is E_i^{tag} , the total field at the tag's antenna is given as the sum of all contributions:

$$E^{tag} = \sum_{i=1}^N \sqrt{G^{tag}(\theta_i^{tag}, \phi_i^{tag})} E_i^{tag} e^{j(2\pi f t + 2\pi r_i / \lambda + \varphi_i)}, \quad (2)$$

where r_i is the distance traveled by the i th ray, and φ_i is the phase shift of the specific contribution due to the reflections on the surrounding walls. $G^{tag}(\theta_i^{tag}, \phi_i^{tag})$ is the gain of the tag's antenna at the angle-of-arrival $\theta_i^{tag}, \phi_i^{tag}$, measured in a spherical coordinate system centered at the tag. λ is the wavelength of operation.

Finally, the power at the tag's chip, P_{tag} is given as

$$P_{tag} = \frac{\lambda^2}{4\pi} \frac{E_{tag}^2}{2\eta} \tau, \quad (3)$$

where τ is the power transmission coefficient, expressing mismatches between the chip's impedance, $Z_c = R_c + jX_c$, and the antenna's impedance, $Z_a = R_a + jX_a$:

$$\tau = \frac{4R_c R_a}{|Z_c + Z_a|^2}, \quad 0 \leq \tau \leq 1. \quad (4)$$

Such a detailed model provides the foundation for accurate characterization of the multipath profile, and thus allows the development of techniques that control propagation effects, as will be demonstrated later.

3. Definition of Coverage

Literally, a point in space is considered to be covered if the modulated backscattered field (from a passive tag at that point) reaches the reader with sufficient power, i.e., with power above reader's sensitivity threshold. Equation (3) defines the power at a passive tag's circuit in the "sleep" state. If that power is strong enough to "awaken" the tag's IC, then the carrier is modulated and backscattered to the reader. This process takes place by changing the tag's load from the "sleep" state to another load's state [17]. The power scattered by the tag at an angle of departure $\theta_{out}^{tag}, \varphi_{out}^{tag}$ is given by

$$P_{sct} = P_{inc} G^{tag}(\theta_{out}^{tag}, \varphi_{out}^{tag}) K_i, \quad (5)$$

where P_{inc} is the incident power at the tag given in Equation (3) for $\tau = 1$. K_i is proportional to the radar cross section of the tag's antenna at modulating state i ($i = 0, 1$), and depends on the load connected to the tag's antenna at state i , the antenna's impedance, and the antenna's structural mode, which is a load-independent quantity [18]. In [17], it was shown that the selection of loads in the two modulating states should take into account the antenna's reflection coefficients and the structural mode, so as to maximize backscatter carrier power per bit, while minimizing the bit-error-rate probability at the reader.

The power that arrives back at the reader's antenna should be calculated by implementing the analytical ray-tracing model presented in Equations (1) and (2), considering the tag to be the transmitter and the reader to be the receiver.

3.1 A Note on the Reader's Sensitivity

In the literature [5, 19], a passive tag is assumed "successfully-identified" if the incident power at the tag is sufficient to power up the tag's IC. The tag-to-reader backscattered power is thus overlooked in the calculations. Such an assumption is valid if the sensitivity level of the reader is much smaller than the backscattered power of any RFID tag marginally operating at the tag's IC sensitivity level. A few years ago, major manufacturers reported a nominal sensitivity value of the chip of -14 dBm, which was measured to be between -11.5 dBm and -12.5 dBm in [19]. Assuming a maximum effective isotropic radiated power (EIRP) of 35 dBm, the maximum path loss from reader to tag is of the order of 48 dB for successful identification of a tag at -13 dBm. In such a case, the mean backscattered power transmitted from the tag is at best of the order of -16 dBm (part of the incident power is used in the rectifier circuit). The power that reaches the reader is approximately -64 dBm. High-end RFID readers have a nominal sensitivity of -77 dBm to -80 dBm [20], hence an adequate margin exists that validates the "successful identification" assumption.

However, significantly improved sensitivity values have been reported recently by major RFID IC chip manufacturers, ranging from -15 dBm [21, 22] down to -18 dBm [23]. An improvement of 5 dB in the sensitivity of the tag is equivalent to 10 dB in the roundtrip of the field, so a backscattered power of -64 dBm would now be -74 dBm, approximating the reader's sensitivity level. Therefore, in the near future, the entire reader-to-tag-to-reader propagation channel must be considered, as identification of a tag could be limited by the reader's sensitivity.

In this paper, we adopt the assumption that the reader's sensitivity level is always smaller than the modulated tag's back-scattered power: the *coverage threshold* is defined by the *desired power* to "awake" the tag's chip, P_{thres} .

At each location, we calculate the received power using the analytical ray-tracing model described before along three orthogonally arranged axes, x , y , z . With the above, the polarization state of the incident field with respect to that of the tag's antenna is taken into account. In Equation (2), we assume $G^{tag}(\theta_i^{tag}, \phi_i^{tag}) = 1$, $\forall \theta_i^{tag}, \phi_i^{tag}$, and in Equation (3), $\tau = 1$. A tag is considered "identified" if the power at the polarization axis of the tag is greater than the tag's threshold. The performance degradation of a tag attached to different surfaces was given in [24], ranging from 1 dB loss for paper or acrylic up to 10 dB for aluminum surfaces.

We define a binary variable, $I_i(P_{thres})$, which describes the identification of a tag with awake threshold P_{thres} at location i :

$$I_i(P_{thres}) = \begin{cases} 1, & \text{if } P_{tag}^i \geq P_{thres} \\ 0, & \text{otherwise} \end{cases} \quad (6)$$

P_{tag}^i denotes the received power at a tag at location i , given by Equation (3). For any tag's threshold P_{thres} , we can estimate the coverage ratio, $C(P_{thres})$, or identification ratio, in any area or

volume of interest and for any polarization of the tag's antenna. We actually consider a dense grid of M points in the volume of interest, and calculate the ratio of the points that are identified, $\sum_{i=1}^M I_i(P_{thres})$, to the total number of grid points:

$$C(P_{thres}) = \frac{1}{M} \sum_{i=1}^M I_i(P_{thres}). \quad (7)$$

4. Estimation Results

The aim is to maximize the coverage in a given volume of interest inside a room, as shown in Figure 1, with commodity RFID hardware. Two circularly polarized antennas were available [25]. One was the MT-242017/NRH, with 10 dBic gain and dimensions of $37 \text{ cm} \times 37 \text{ cm}$, and the other was the MT-242032/NRH, with 7 dBic gain and dimensions of $19 \text{ cm} \times 19 \text{ cm}$. The radiation patterns with the half-power beamwidths of the two antennas are given in Figure 2.

4.1 Representative Results

The 10 dBic-gain antenna was considered at $x = 1.5 \text{ m}$, $y = 0.1 \text{ m}$, $z = 2 \text{ m}$, tilted with an angle of 20° , as shown in Figure 2. The transmission power was set to 30 dBm at a frequency of 865 MHz. The walls were modeled as single-layer reinforced concrete walls of 40 cm thickness, with $\epsilon_r = 6.5$ and $\tan \delta = 0.287$ [14]. The power was calculated in the entire room on the tips of an orthogonal grid with a 10 cm spacing. The received powers for a z -polarized tag along a z slice, a y slice, and an x slice are shown in Figures 3a-3c, respectively. Similar results were extracted for the x - and the y -polarized field for any cut inside the room. By com-

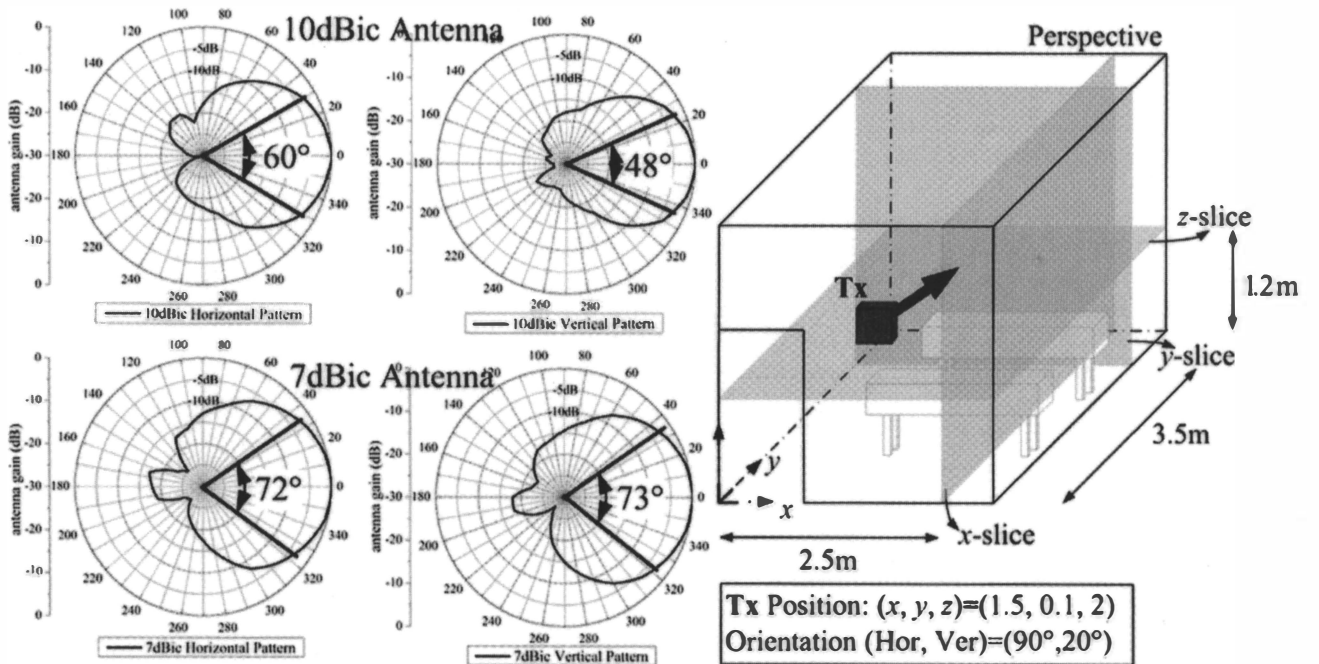


Figure 2. A representation of a single-antenna configuration and the radiation patterns of the available antennas.

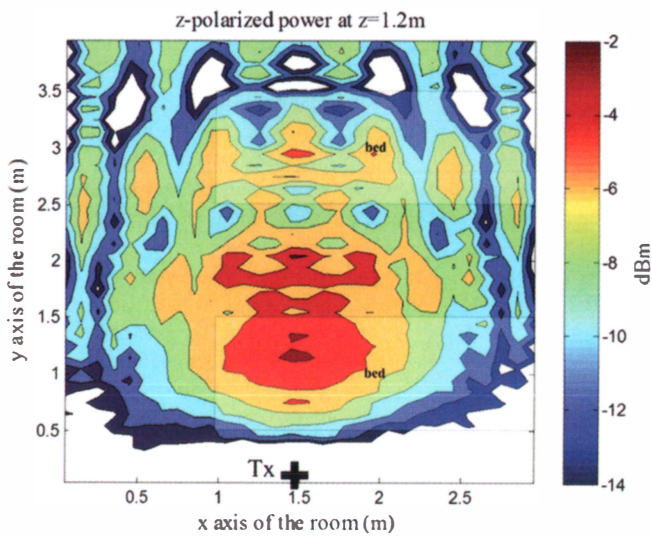


Figure 3a. The received power for a z-polarized tag at $z = 1.2$ m.

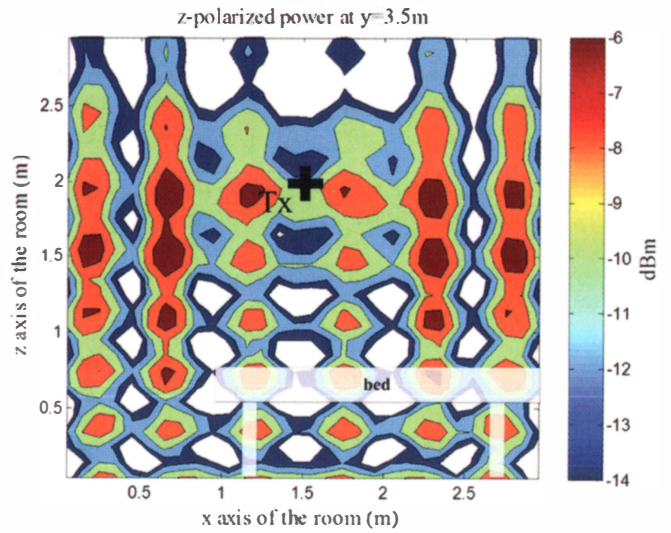


Figure 3b. The received power for a z-polarized tag at $y = 3.5$ m.

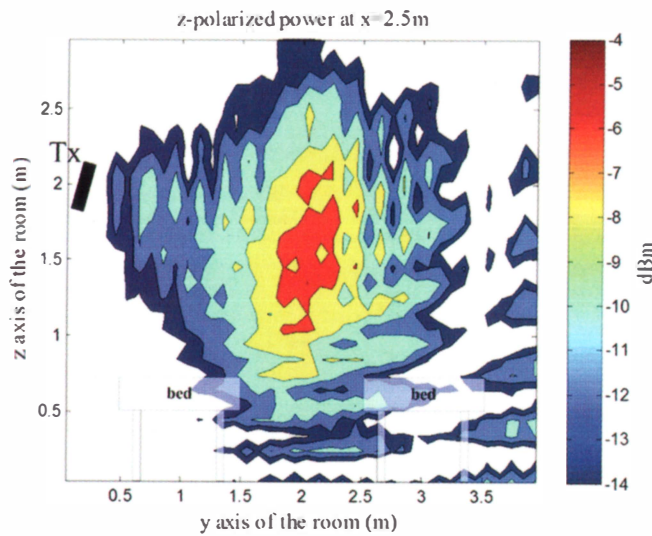


Figure 3c. The received power for a z-polarized tag at $x = 2.5$ m.

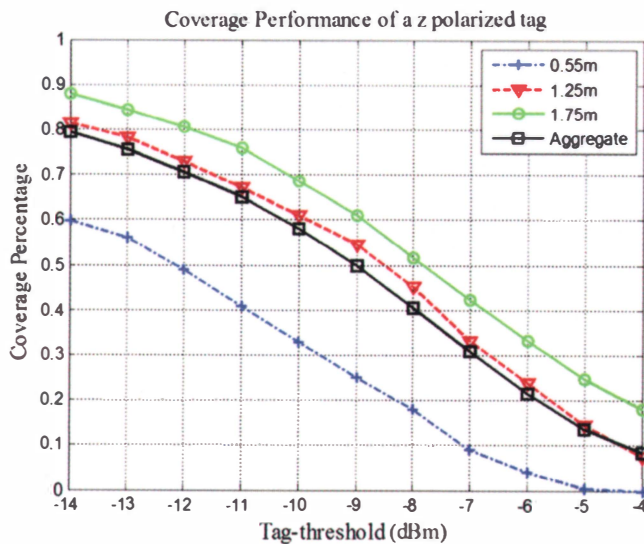


Figure 3d. The coverage performance of a z-polarized tag at three heights as a function of increasing the tag's threshold.

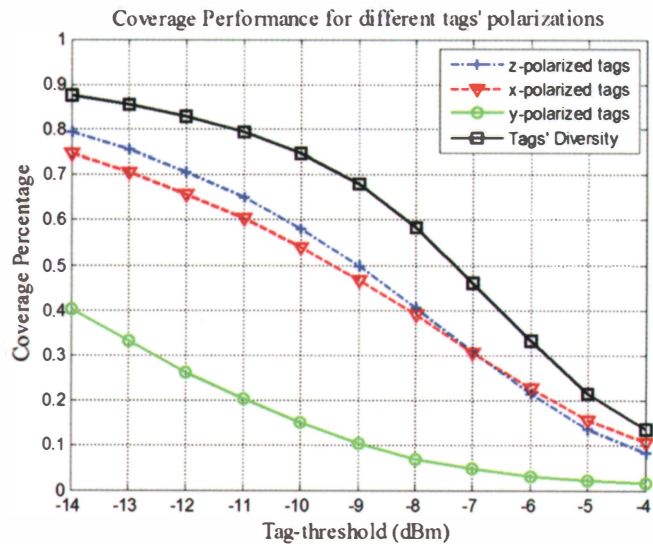


Figure 3e. The coverage performance of z-, x-, and y-polarized tags as a function of the tags' diversity.

binning these results, one could identify the dominant propagation mechanisms responsible for the field's interference patterns inside the room, due to multipath, and then properly move the antenna inside the room, manipulating the resulting field as desired.

As discussed in the previous section, coverage plots were formed by processing the power results, as defined in Equation (7). In Figure 3d, coverage curves for z -polarized tags are given at three selected heights – 0.5 m, 1.2 m, and 1.8 m above the ground – as well as aggregate results in the entire volume of interest. Coverage was evaluated at several heights, as we sought balanced performance over the entire volume of interest. In Figure 3e, aggregate coverage results are given for x -, y -, and z -polarized tags. The performance for a y -polarized tag was significantly worse than the performance for an x - or a z -polarized tag because the reader antenna's circular polarization was distributed mainly along the x - z plane. The field along the y axis resulted mainly from the 20° down-tilt of the antenna for the configuration of Figure 2. In the same plot, coverage performance is also evaluated for a case of "Tag Diversity," explained below.

4.2 Tag Diversity

Asset-tracking involves several objects, e.g., wheelchairs and infusion pumps in a hospital. Benefiting from the tags' low cost and small dimensions, we can associate more than a single tag with each object. To examine the case of diversity, we assumed an x -, a y -, and a z -polarized tag attached to each object. In each location, successful identification was guaranteed if at least one of the three tags was powered up. Aggregate coverage increased by 10% at the -14 dBm threshold, reaching 89%, compared to the single z -polarized tag, as shown in Figure 3e. Even better improvement was recorded at a greater tag threshold. Notice that this type of diversity was different than the multiple-tags case analyzed in [4], where all tags were assumed to share the same ID, and thus modulated the reader's signal in the same manner.

4.3 Planning Rules for Antenna Selection and Placement Applicable to any Room

As a basic planning rule, the reader's antenna(s) should be installed *within* the volume of interest. Otherwise, part of the transmitted power in the vicinity of the reader is wasted in a volume where tags are not expected. As a consequence, antenna placement centrally on the ceiling should be avoided. In addition, in the volume of interest the radiated field of any ceiling patch antenna is expected to be polarized along the xy plane, thus failing to identify z -polarized tags. Even if a ceiling antenna includes z -polarized elements, a null is expected below the antenna, hence within the volume of interest, for the corresponding z -polarized field. Expected tag polarization when attached to target equipment should be carefully considered during the planning process. Overlooking this factor could result in poor performance, even in the vicinity of the reader's antenna.

Implementation of omnidirectional antennas in RFID systems is usually impractical. Such antennas demand inconvenient placement in the center of the volume of interest, so that all energy would be efficiently radiated.

As a consequence, the most convenient locations for reader antenna(s) placement inside the volume of interest are the vertical

walls. Hence, single-lobe directive antennas represent the obvious choice. It is noted that a vertically polarized antenna must be tilted in order to introduce fields along the horizontal plane. Tilting implies that the antenna *must* be installed at a certain height so that the radiation pattern illuminates the volume of interest. Instead, a circularly polarized antenna radiates in the vertical and the horizontal planes without tilting. From such a perspective, this type of antenna allows for greater flexibility in terms of placement.

Focusing on antenna-placement along a vertical wall, consider the antenna of Figure 2, moved close to the vertical edge of the room, e.g., at $x = 0.1$ m, and away from the center of the wall. A strong, first-order reflection is introduced by the adjacent wall (to the left of the antenna, for example), due to the corresponding shallow grazing angle of the incident field. As the strong reflected field interacts with the direct field, it introduces deep fading in the vicinity of the wall. Even if a corner-placed antenna is properly tilted towards the room's interior, fading still exists, since the geometrical conditions are unaltered: it is simply exhibited at smaller power levels.

Therefore, *reader antenna(s) should be placed away from corners, centrally on the surface of the vertical walls, so that the volume of interest is illuminated.*

Depending on the actual dimensions of the room, an antenna with a proper radiation pattern should be selected. A single-lobe antenna with 3 dB horizontal and vertical beamwidths, denoted as $\Delta\varphi_{3dB}$ and $\Delta\theta_{3dB}$, respectively, has a gain expressed by $G(\text{dB}) = 10 \log_{10} \{K / (\Delta\theta_{3dB} \Delta\varphi_{3dB})\}$ [18]. By substituting the values for $\Delta\varphi_{3dB}$, $\Delta\theta_{3dB}$, G (in dBic) of the available MTI antennas [25] in the above formula, we derived a value of $K \approx 27570$, which yields an error of ± 0.2 dB.

To evaluate the desired antenna's gain, one must estimate the desired received power for a linearly polarized tag located at the most distant point from the antenna in the volume of interest. Hence, the antenna's desired gain can be evaluated by substituting the desired received power, P_r , in the Friis free-space formula, and then solving for the reader's antenna gain, G , assuming a known maximum transmission power, e.g., 1 W. A suitable value for P_r is $P_r = P_{thres} + L_{pol} + L_{pat}$, where L_{pol} denotes polarization mismatches (3 dB is recommended), and L_{pat} denotes the absolute difference of the antenna's gain at the direction of the receiver minus the maximum antenna gain (again, 3 dB is a reasonable value). Having calculated the desired antenna gain, parametric curves with the variation of $\Delta\varphi_{3dB}$ and $\Delta\theta_{3dB}$ can be constructed. For example, for a maximum distance of 5 m, a transmission power of 30 dBm, $P_r = -14 \text{ dBm} + 6 \text{ dB} = -8 \text{ dBm}$. At an operating frequency of 865 MHz, the desired reader antenna's gain is $G = 7.16 \text{ dBic}$. Parametric curves with the variation of $\Delta\varphi_{3dB}$ with respect to $\Delta\theta_{3dB}$ for three antenna gains are given in Figure 4. Depending on the volume of interest, one should select an antenna with the most appropriate pattern, and then select a commercially available antenna that best matches the desired characteristics. For example, if the height of the volume of interest is small, say 1 m (ranging from 1 m to 2 m in height), $\Delta\theta_{3dB} = 50^\circ$ can be selected, thus allowing for a wider $\Delta\varphi_{3dB} = 110^\circ$. This assures better coverage to the left and to the right of the antenna's boresight. The characteristics of the two available antennas are marked in Figure 4.

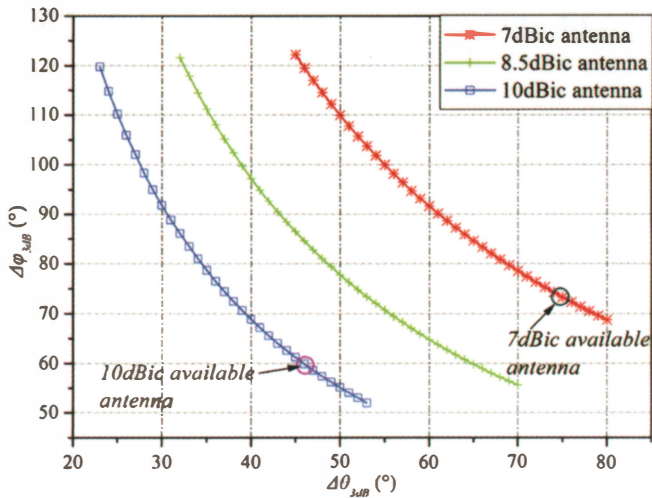


Figure 4. The variation of the horizontal as a function of the vertical 3 dB beamwidth of single-lobe circularly polarized antennas with different typical gains.

If the volume of interest is not adequately covered by a single antenna, multiple antennas can be selected, as analyzed in Section 5.

4.4 A Note on Parameters not Considered in the Model that Influence the Field Inside the Room

In an operational room, furniture or other equipment exists inside the room, thus influencing the distribution of the field in the volume of interest. Such scatterers are expected to introduce minima and maxima in their vicinity, where the direct field could be comparable to the introduced scattered field. The size of the induced variations with respect to the estimated field pattern of an empty room greatly depends on the electromagnetic and geometrical properties of the scatterers. For example, a plastic board hung on a wall is expected to have a negligible effect, whereas a metallic table will strongly affect the field in its neighborhood. In addition, moving people are expected to influence the field, when present.

Misplacement and movement of the aforementioned scatterers can be treated as different states of a Markov chain. At each state, all objects of interest are considered at fixed locations, and the field is analytically computed, either by a ray-tracing technique or other methods from computational electromagnetics.

4.5 Actual Field Compared to Free-Space Estimation

A comparison is presented below between the coverage performance of a system operating in “free-space” conditions and one operating in “real” multipath conditions, for the same calculation volume. The received power of a z-polarized tag along a y slice at 3.5 m for the configuration of Figure 2 is presented in Figure 5a. This result is compared with the corresponding estimations of the actual field given in Figure 3b. Multipath creates both constructive and destructive interference patterns. The former results in covered

areas at greater distances compared to free space, but the latter leads to minima and “holes” in the field’s pattern inside the room, which limit the reliability of the reader’s read-region at any distance.

Better coverage was recorded when considering the actual field over free-space conditions (Figure 5b). In free-space conditions, coverage at any point was calculated deterministically by Equations (6) and (3), taking into account the radiation pattern of the antenna, resulting in a *strictly bounded* coverage volume around the reader’s antenna. In multipath conditions, coverage depends on the locations of the walls, as well as on unknown parameters, such as the electromagnetic properties of the walls. Covered areas arise beyond the “free-space bounded volume” due to constructive summation of the direct field with scattered components. A statistical analysis is carried out below.

Equations (6) and (7) state that the coverage ratio for a given threshold grows as the power in the volume of interest grows. It is

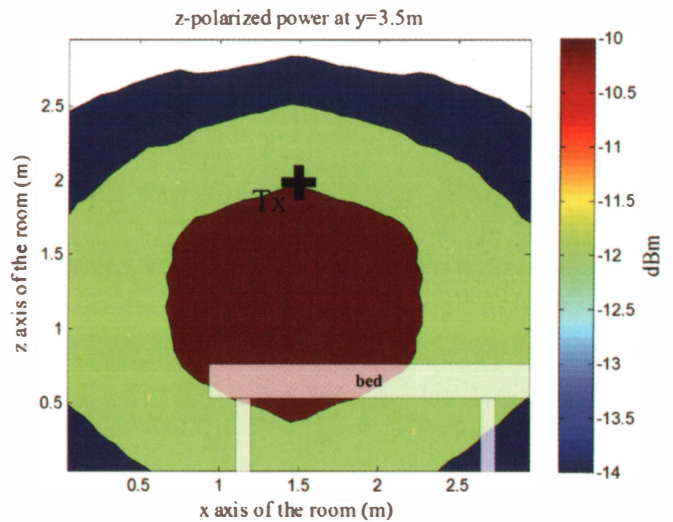


Figure 5a. The received power for a z-polarized tag at y = 3.5 m, assuming free-space conditions.

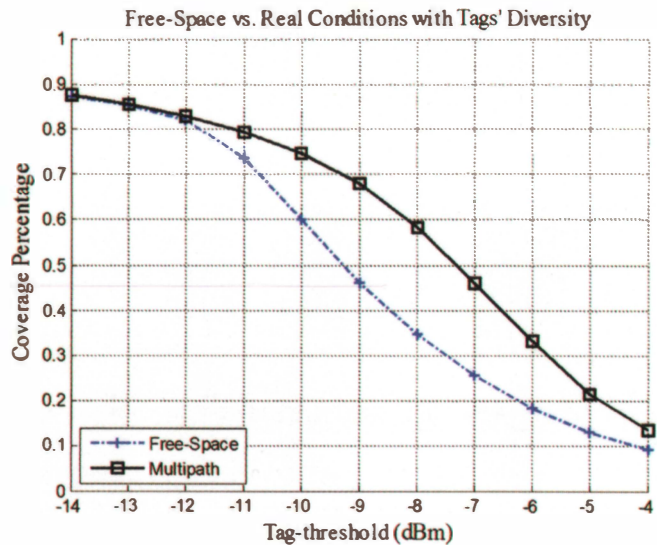


Figure 5b. The coverage performance assuming free-space conditions as a function of the actual field, considering three orthogonally polarized tags at each location.

shown below that the mean expected power at each position inside a room is greater than the corresponding power calculated in free-space under the following conditions:

1. The line-of-sight (LOS) field is not obstructed for any point inside the volume of interest.
2. The phases of the different field contributions can be regarded as independent random variables, uniformly distributed in $[0, 2\pi]$.

Let E_0 denotes the field at a random location inside a room due to the direct contribution, and let E_i denote the i th of the M reflected/scattered contributions arriving at the same location with phase θ_i . The total field, E , is

$$E = \underbrace{E_0 e^{j\theta_0}}_{\text{LOS}} + \underbrace{\sum_{i=1}^M E_i e^{j\theta_i}}_{\text{Reflected/Scattered}}. \quad (8)$$

The power, P , is proportional to the square of the electric field:

$$\begin{aligned} P \sim |E|^2 = EE^* &= \left(\sum_{i=0}^M E_i e^{j\theta_i} \right) \left(\sum_{i=0}^M E_i e^{-j\theta_i} \right) \\ &= \sum_{i=0}^M E_i^2 + 2 \sum_{i \neq j} E_i E_j \cos(\theta_i - \theta_j). \end{aligned} \quad (9)$$

The phase, θ_i , of each field contribution is treated as an independent random variable uniformly distributed in $[0, 2\pi]$. Let φ be a random variable, defined as

$$\varphi = \theta_i - \theta_j. \quad (10)$$

It can be shown that the probability density function of φ , specified by the proper convolution of the probability density functions (pdfs) of θ_i, θ_j , is given as [26]

$$f_\varphi(x) = \begin{cases} 1/(2\pi)^2 (2\pi + x), & -2\pi \leq x \leq 0 \\ 1/(2\pi)^2 (2\pi - x), & 0 < x \leq 2\pi \\ 0, & \text{otherwise} \end{cases}. \quad (11)$$

The mean expected power, $E[P]$, of Equation (9) is given as

$$\begin{aligned} E[P] &\sim E \left[\sum_{i=0}^M E_i^2 + 2 \sum_{i \neq j} E_i E_j \cos(\theta_i - \theta_j) \right] \\ &= \sum_{i=0}^M E_i^2 + 2 \sum_{i \neq j} E_i E_j E[\cos(\phi)]. \end{aligned} \quad (12)$$

From Equation (11), it can be shown that $E[\cos(\phi)] = 0$. Therefore,

$$E[P] \sim \sum_{i=0}^M E_i^2 = \underbrace{E_0^2}_{\text{LOS}} + \underbrace{\sum_{i=1}^M E_i^2}_{\text{Reflected/Scattered}} \geq \underbrace{E_0^2}_{\text{LOS}}. \quad (13)$$

Hence, if the line-of-sight contribution is not obstructed, and the phases of the scattered/reflected components can be considered as independent random variables uniformly distributed in $[0, 2\pi]$, then the *mean* expected power at any location inside the room is equal to or greater than the free-space direct field. Equality holds when the scattered field is zero.

5. One-Reader-Antenna Compared to a Two-Reader-Antenna Configuration

5.1 Single-Antenna Configurations

We considered any of the available transmitting antennas at the center of one of the walls, as it is shown in Figure 2. Part of the volume of interest could not be covered, because of the narrow 3 dB beamwidth of the horizontal radiation patterns of the available antennas. Even worse performance was recorded by placing the antennas at the corners of the room for several heights and tilting selections, for the reasons analyzed in Section 4.3. The idea of implementing two antennas instead of one in various configurations was then tested as a preferable solution.

5.2 Double-Antenna Configurations

Double-antenna configurations are shown in Figure 6. The two antennas are fed via a 3 dB bidirectional power splitter/combiner. As a result, each antenna transmits at a 3 dB smaller power level (27 dBm) than does a single-antenna configuration. Hence, a fair comparison with the single-antenna configurations can be carried out, given that the same amount of power is radiated inside the room. In addition, as the antennas are to be installed inside a patient's room, two MT-242032/NRH antennas with 7 dBi gain were selected, due to their significantly reduced dimensions compared to the 10 dBi antennas. The EIRP per antenna and per excitation axis was 31 dBm, smaller than the maximum limit in Europe. In the following results, the threshold was set to -11 dBm, instead of -14 dBm, in order to account for the 3 dB reduction of power per antenna, while the transmitted power was preserved at 30 dBm.

An important property of the double-antenna configurations is demonstrated in Figure 7. The power along a z slice at 1.2 m for a z -polarized tag for Configuration 2 is given. The hyperbolas drawn in Figure 7 represent the geometric space of the points where the direct fields from the two antennas contribute with π phase difference, and hence add destructively:

$$|d_1 - d_2| = (2k + 1)\lambda/2, \quad k = 0, 1, \dots, \quad (14)$$

where d_1, d_2 denote the corresponding distances from the two sources, and λ is the wavelength in free space. Depending on the magnitude of each direct contribution, the minimum could be so

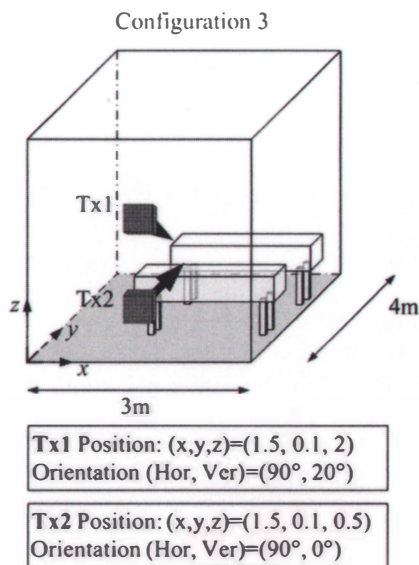
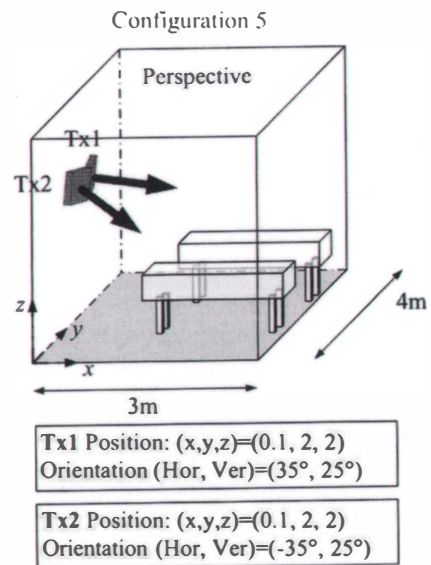
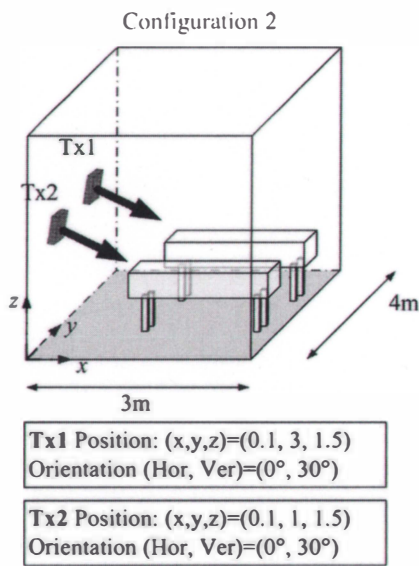
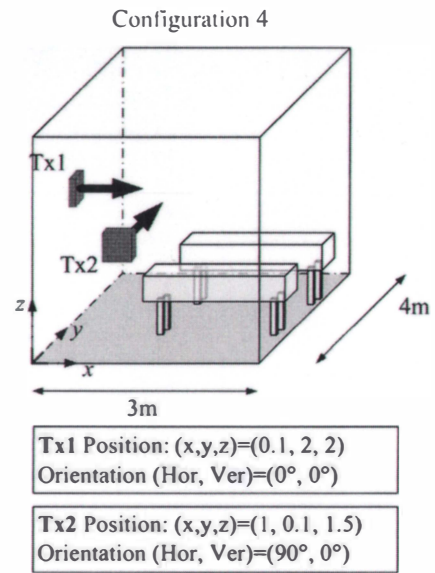
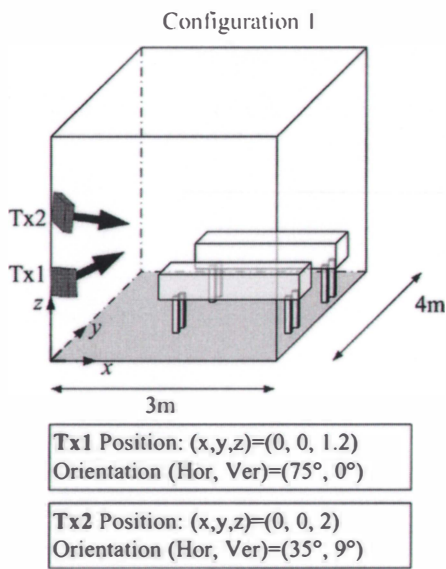


Figure 6 (continue). Representations of the double-antenna configurations.

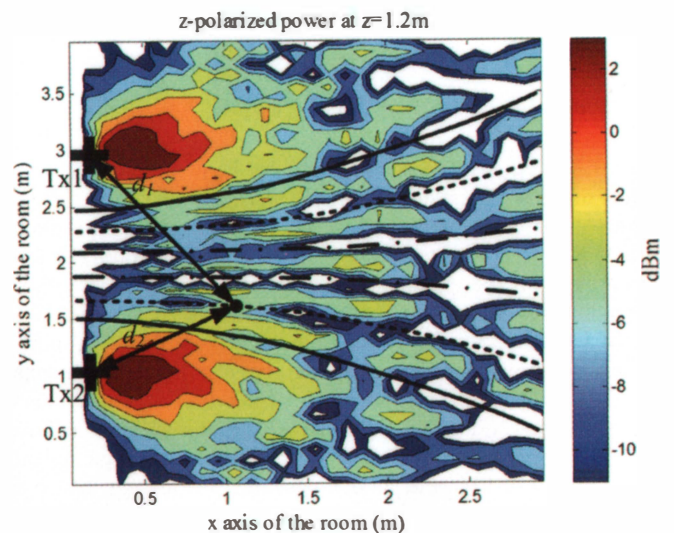


Figure 6. Representations of the double-antenna configurations.

Figure 7. The received power for a z-polarized tag at $z=1.2\text{m}$ for Configuration 2.

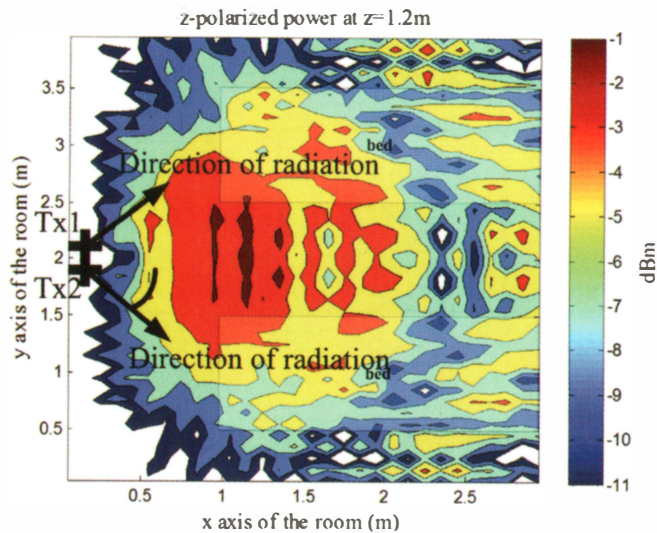


Figure 8. The received power for a z-polarized tag at $z = 1.2$ m for Configuration 5.

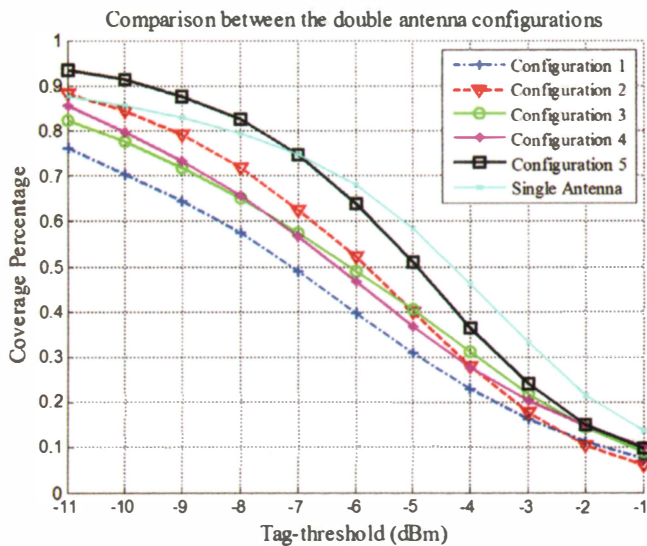


Figure 9. The coverage performance for the five double-antenna configurations, assuming tag diversity.

large that a tag at this location could not be identified, despite its small distance from the two antennas. Similar results were extracted for Configurations 1, 3, and 4. Deep fading was introduced at predictable locations determined by Equation (14), depending on the positions of the two antennas. Therefore, “directing the two antennas towards the volume of interest” is not a sufficient condition for coverage maximization. On the contrary, “holes” were introduced, even in the vicinity of the two antennas, due to destructive summation of the strong direct contributions of the antennas. The corresponding coverage ratio, defined in Equation (7), was worse than the coverage ratio for the single-antenna configuration of Figure 2, as demonstrated in Figure 9. However, the predictability of the arrangement of the “holes,” described by Equation (14), can be exploited when a minimum is desired at a specific region, e.g., the sensitive volume of the patient’s body above each bed.

For coverage maximization, the two antennas must be placed so that:

1. The power from each antenna is radiated towards the volume of interest.
2. Each of the two antennas illuminates a different part of the volume of interest, so that destructive summation of the direct fields from the two antennas is small.

These constraints were well satisfied by Configuration 5, shown in Figure 6. The two antennas illuminated different parts of the room, making sure that the 3 dB horizontal beamwidths of each of the antennas radiated into different angular segments. A z slice at 1.2 m of the z -polarized received power is shown in Figure 8.

The coverage performance of all five configurations of Figure 6 is shown in Figure 9. Configuration 5 ensured 93% coverage at -11 dBm. Notice that Configuration 1 recorded a poor 77% coverage, due to destructive-interference effects. By comparing the coverage performance of Configuration 5 with the corresponding performance for the single-antenna configuration, also shown in Figure 9, a better coverage percentage was accomplished at the expected tags’ thresholds, despite the fact that each of the two antennas radiated at a 3 dB smaller power level. The reason was that the transmitted power was better directed towards the volume of interest.

6. Coverage Improvement

Despite the fact that 93% coverage was accomplished with a double-antenna configuration, fed via a 3 dB splitter, it was found that all other double-antenna configurations suffered from destructive-interference effects, causing severe degradation of the coverage performance of the system. It was shown that directing the power towards the volume of interest is not a sufficient condition for effective planning. Control of destructive-interference effects represents an equally important parameter of the problem. In any case, the expected coverage performance remains vulnerable to technicians’ installation errors, tags’ inferior performance when attached to the tracked object [24], etc. In this section, different solutions are proposed, aimed at the maximization of the coverage performance by introducing active devices in the configuration, while abiding by the maximum EIRP constraints.

6.1 Introduction of a Phase Shifter

The potential to introduce a device capable of eliminating or minimizing the destructive-interference effects was investigated. As discussed earlier, the two antennas introduced “holes” in the surrounding area, based on the magnitude and the phases of the transmitted fields. The desired task is to “control” the locations of the holes and properly “move” them inside the room.

Consider the direct field at receiving location A from the two antennas Tx_1 and Tx_2 , positioned at random places inside the room, as demonstrated in Figure 10. Let E_1 with phase φ_1 be the field at a tag located at A from Tx_1 , and let E_2 with phase φ_2 be the field at the same tag from Tx_2 . Assuming that the two antennas radiate in phase, we have $\varphi_1 = 2\pi r_1/\lambda$ and $\varphi_2 = 2\pi r_2/\lambda$,

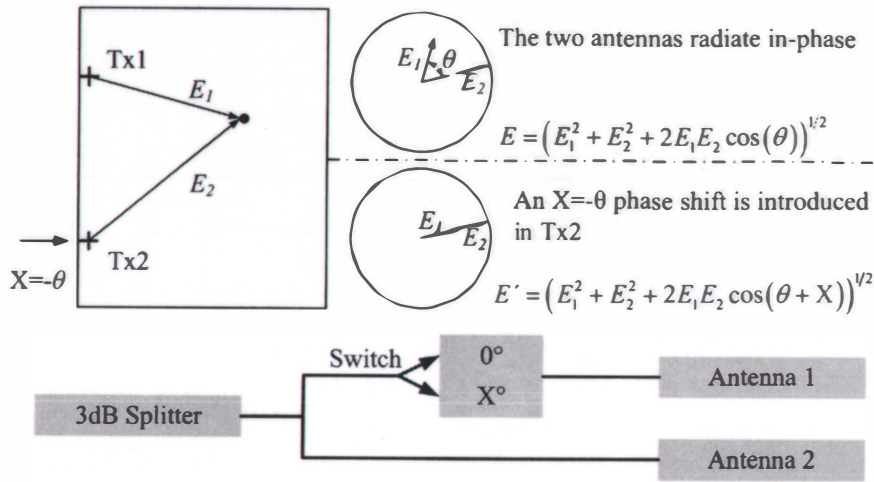


Figure 10. Introducing a switch-controlled phase shift in the feeding of one antenna.

where r_1, r_2 are the path lengths from Tx_1 and Tx_2 to A, respectively. The two contributions can be represented as two vectors with magnitudes E_1, E_2 , respectively, forming an angle $\theta = \varphi_1 - \varphi_2$, as shown in Figure 10 (top right). The magnitude of their sum is

$$E = \left[E_1^2 + E_2^2 + 2E_1E_2 \cos(\varphi_1 - \varphi_2) \right]^{1/2} \quad (15)$$

$$= \left[E_1^2 + E_2^2 + 2E_1E_2 \cos(\theta) \right]^{1/2}.$$

Notice that when exciting Tx_2 with an X phase delay with respect to Tx_1 , the phase difference at A becomes $\theta' = \varphi_1 - \varphi_2 + X = \theta + X$. The field at A is then given by

$$E' = \left[E_1^2 + E_2^2 + 2E_1E_2 \cos(\theta + X) \right]^{1/2}. \quad (16)$$

By selecting $X = \pm\pi$, we have $\cos(\theta \pm \pi) = -\cos(\theta)$: hence, destructive interference becomes constructive. We propose the introduction of a switch, as shown in Figure 10 (bottom), which controls the feeding of one of the antennas. It either does not insert a phase delay and hence the two antennas radiate in phase, or it does introduce a π phase shift. In the two states of the switch – assuming that all other conditions such as the transmission power, propagation conditions etc., are unaltered – the field at a random position inside the room is then given by Equations (15) and (16), respectively. A tag is identified if it is powered up in at least one of the two states of the switch. By introducing additional phase shifts, e.g., $\pm\pi/2$ (Figure 11), the maximum of the cosine term, shown in black-dotted line, always takes large positive values, leading to greater combined fields in the volume of interest at the expense of greater complexity of the switching system.

Even though the proposed method exploits principles of traditional antenna-array synthesis, [27-30], where beamforming is accomplished by properly phase shifting the excitations of discrete elements, some key differences are noted:

1. No specific beam pattern is sought. As long as a π phase shift is introduced, then a minimum in one state of the switch becomes a maximum in the other state.

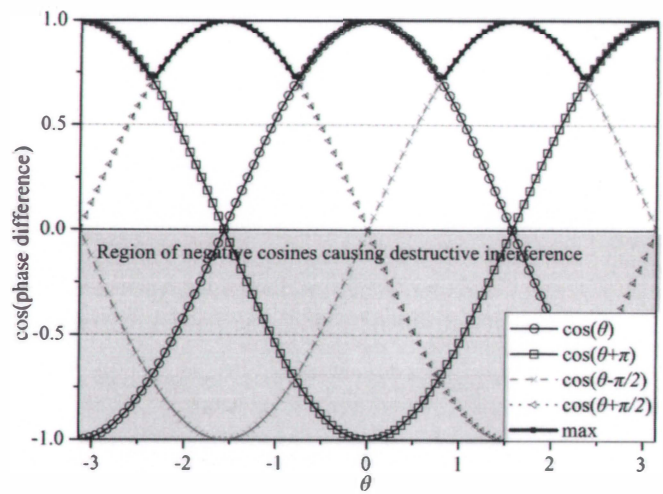


Figure 11. The variation of the cosine term for several phase shifts. The maximum of the resultant cosine term is also shown.

Therefore, simplicity and ease of installation are insured.

2. The antennas need not be placed close to each other. Instead, they can be distributed anywhere in the volume of interest, e.g., on opposite vertical walls inside the room. In such a case, we cannot define the double antenna's radiation pattern in the volume of interest, because the latter lies between the two antennas. In traditional antenna-array theory, the radiation pattern is evaluated on the surface of a sphere centered at the array, enclosing it.

We have repeated the simulations for the five double-antenna configurations shown in Figure 6 by considering the introduction of a single phase shift equal to π . The results are shown in Figure 12. By comparison with Figure 9, the coverage performance of the system was boosted, reaching at least 93% in all cases. It is interesting that nearly identical performance was recorded for all configurations. The importance of the introduction of the proposed phase shifter is that coverage is no longer vulnerable to installation errors or the need for careful fine-tuning of processes. Instead, it

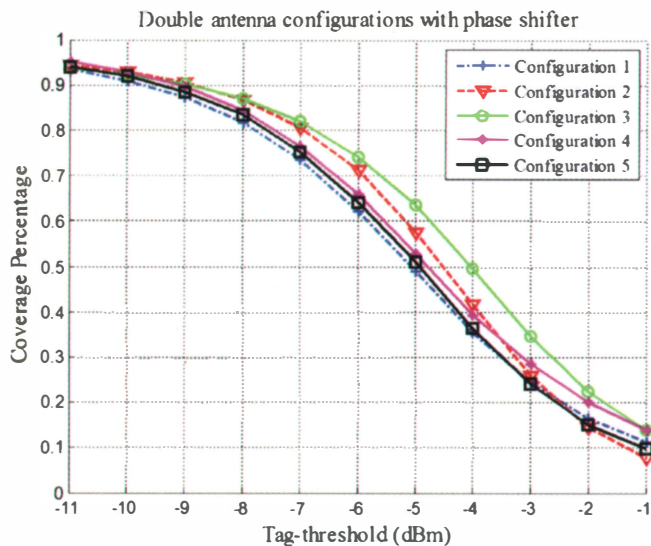


Figure 12. The coverage performance of the five double-antenna configurations, after the introduction of the proposed switch-controlled phase shift $X = -\pi$.

seems that good performance is accomplished anywhere you place the antennas inside the room, as long as they both radiate towards the volume of interest. The switching phase shifter then eliminates destructive interference patterns.

It must be emphasized that the insertion of the phase shifter can eliminate destructive interference effects caused by *different sources* (two antennas herein), and not effects created by the multipath of a single antenna configuration. The reason is that by inserting a phase delay in a single antenna configuration, the same delay is physically inserted in all multiple-reflected/scattered components that reach the tag. The same phase differences are thus preserved among the different components that constitute the total field. Therefore, introduction of a switch-controlled phase shifter represents an option only when multiple transmitting antennas are involved.

6.2 Alternative Transmission of Multiple Antennas

Another possibility for improving the performance of the system is to implement two antennas, but to schedule their transmissions in different timeslots. As a consequence, there will be no interaction between them. The benefit is twofold: 1) the 3 dB losses of the passive splitter are avoided, and thus all the power is transferred to the active transmitting antenna; and 2) the implementation of two antennas instead of one allows better directing of the transmitted power towards the volume of interest. The results for the five configurations of Figure 6 are shown in Figure 13. Better performance was recorded in three cases (Configurations 2, 4, and 5), and worse performance occurred in the other two cases (Configurations 1 and 3), compared to the results of Figure 12.

6.3 Phase Shifter Combined with a Power Amplifier

Finally, we have repeated the simulations including the introduction of the π phase shifter, assuming in addition a 3 dB power

amplifier to compensate for the passive-splitter losses. In terms of maximum allowable radiated power, it is possible to introduce such an amplifier, since the EIRP per antenna remains smaller than the corresponding limit. The results are shown in Figure 14. The best coverage performance was accomplished, reaching a maximum close to 98% coverage. Coverage remained above 90%, even at -10 dBm. All configurations demonstrated similar performance because of the switch-controlled phase shifter, as discussed earlier.

7. Measurements

Distributed tag measurements along a given surface were reported in [31-33]. In [31, 32], the authors validated a stochastic $M \times L \times N$ reader-to-tag-to-reader propagation model [4], where M

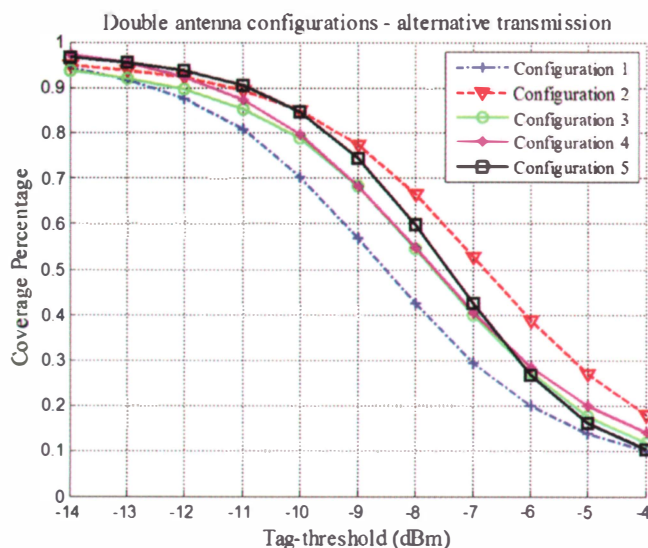


Figure 13. The coverage performance of the five double-antenna configurations, assuming that the two antennas did not transmit simultaneously.

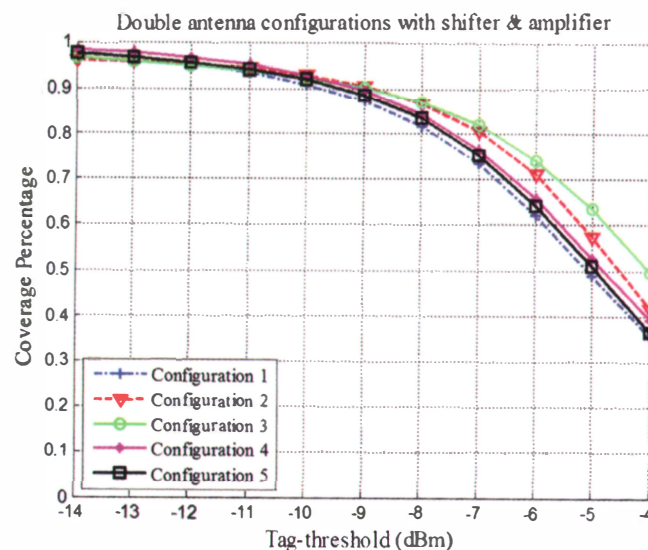


Figure 14. The coverage performance of the double-antenna configurations, assuming a switch-controlled phase shifter plus a 3 dB power amplifier.

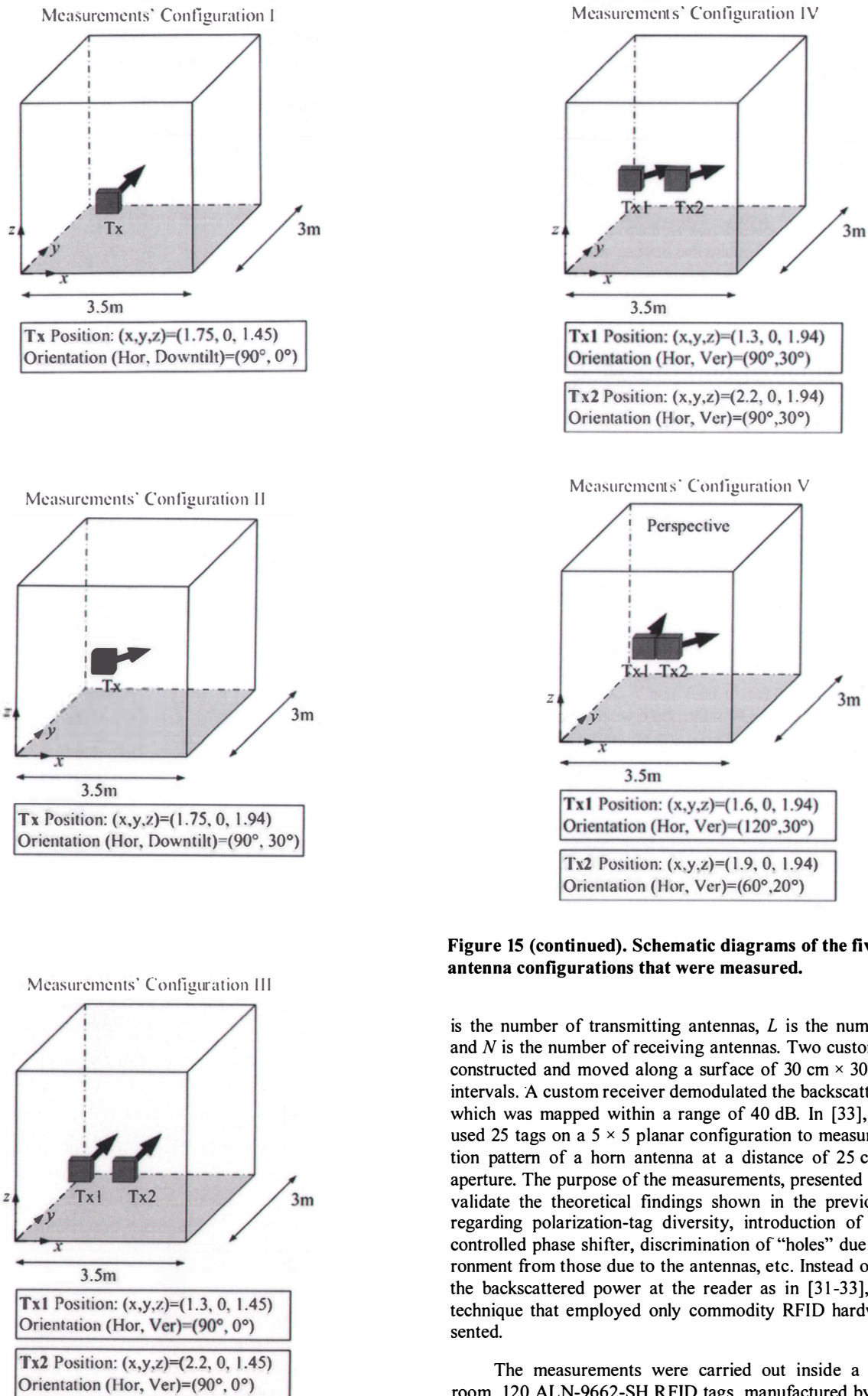


Figure 15 (continued). Schematic diagrams of the five different antenna configurations that were measured.

is the number of transmitting antennas, L is the number of tags, and N is the number of receiving antennas. Two custom tags were constructed and moved along a surface of $30\text{ cm} \times 30\text{ cm}$ at 1 cm intervals. A custom receiver demodulated the backscattered power, which was mapped within a range of 40 dB . In [33], the authors used 25 tags on a 5×5 planar configuration to measure the radiation pattern of a horn antenna at a distance of 25 cm from the aperture. The purpose of the measurements, presented next, was to validate the theoretical findings shown in the previous sections regarding polarization-tag diversity, introduction of the switch-controlled phase shifter, discrimination of “holes” due to the environment from those due to the antennas, etc. Instead of measuring the backscattered power at the reader as in [31-33], a different technique that employed only commodity RFID hardware is presented.

The measurements were carried out inside a $3.5\text{ m} \times 3\text{ m}$ room. 120 ALN-9662-SH RFID tags, manufactured by Alien [34], were hung at two levels: at heights of 130 cm and 185 cm above the floor, equally spaced at 50 cm intervals along the x, y, z axes, as represented in Figure 16 and photographed in Figure 17.

Figure 15. Schematic diagrams of the five different antenna configurations that were measured.

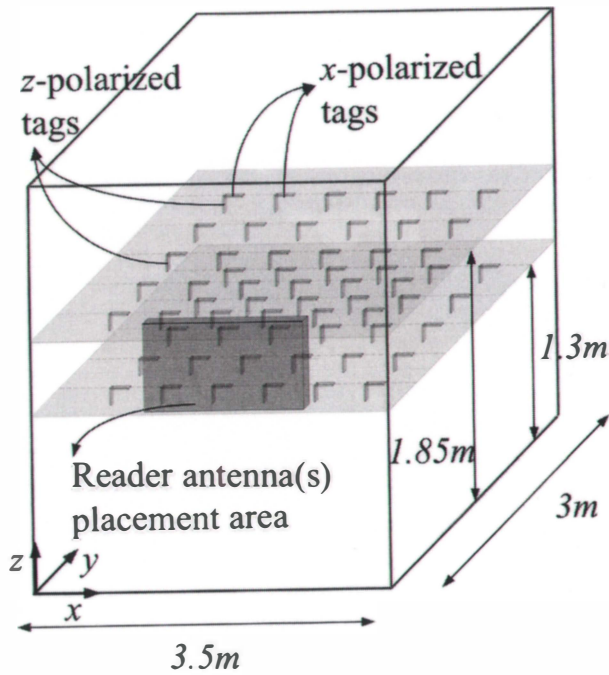


Figure 16. The setups for the measurements and the tags' locations.

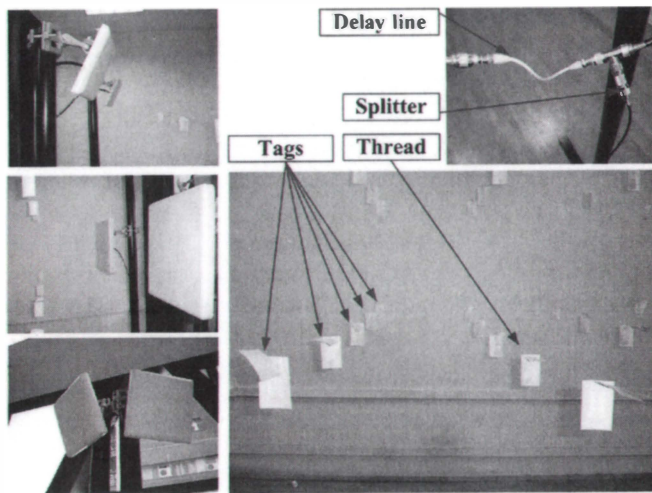


Figure 17. The tags formed a three-dimensional measurement grid for the x - and z -polarized components of the transmitted field.

Two tags were suspended side-by-side at each position by using a cotton string: one was vertically polarized and the other was horizontally polarized along the x axis. The ALN-9662-SH tag was powered by Alien's Higgs 3 UHF RFID IC, which has a nominal "sensitivity during read" threshold of -18 dBm [23]. The radiation pattern of the tag's antenna is similar to that of a dipole, and was given in [34]. Each tag's location along with its unique ID was stored in a database. Hence, when a tag's ID was read by the RFID reader, the location of the specific tag in the room was retrieved from the database.

The Speedway IPJ-R1000 UHF Gen2 RFID tag reader [20] was connected to the transmitting antenna(s) via a single antenna port. The reader's transmission power was reduced from 30 dBm to 15 dBm in steps of 1 dB at 4 s intervals. The 4 s period was

selected as it was found experimentally that it represented a sufficient timeframe for all 120 installed tags to be identified, provided that the power level at each tag's IC was sufficient.

Five different antenna configurations were measured, as shown in Figure 15. For each configuration, both available antenna types were installed and measured. All double antenna configurations were measured twice: with and without a delay line connected to the feeding of Tx_1 , as shown in Figure 17 (top right), thus measuring the performance of the proposed phase shifter. The length of the delay line was equal to 13 cm, approximating the desired 180° phase delay in the feeding of one of the antennas, assuming a typical refractive index of the line approximately equal to 1.4 with respect to free space at the operating frequency of 865 MHz. The losses of the reader-antenna feeding cable were measured to be 0.6 dB. The additional losses of the delay line were 0.1 dB. The available power splitter had an insertion loss of 4 dB (in addition to the 3 dB coupling loss per antenna). The typical insertion losses for a commercial low-cost quality splitter are less than 0.2 dB [35].

Two types of measurement results were extracted: propagation results and coverage results.

7.1 Propagation Results

The idea was to use the tags in order to measure the power level of the signal transmitted by the reader at each tag, and thus create three-dimensional power plots inside the measurement volume. One method would be to measure the received backscattered power at the reader, and to then calculate the power at the tag, provided 1) that a known injective (one-to-one) function that relates the incident field at the tag's antenna to the modulated field radiated by the tag's antenna exists; and 2) that the channel is stationary within the incident-to-backscattered time period. However, such an injective function cannot be defined, due to the limiter at the output of the rectifier's circuit: the limiter affects the input impedance of the tag's chip for large incident power levels, and thus the modulated backscattered power [36, pp. 101-103].

Another method would be to exploit the constant tag's "sensitivity-during-read" threshold. By reducing the reader's transmitted power, T , from $T_{max} = 30$ dBm to 15 dBm, we could identify the minimum transmission power level, T_i^{min} , $i = 1, \dots, 60$, for which each of the 60 installed tags, per axis of polarization, was identified. Since we know that at T_i^{min} , the power at the i th tag's IC, P_{thres}^{IC} , was -18 dBm [23], we could estimate the corresponding received power, P_{thres} , at the location of the tag and for the tag's polarization axis. As explained in Section 2 and expressed in Equations (2)-(4), the power at the tag's IC represented the total contribution of multipath components arriving from different directions. Each component's field could not be measured. The product of the tag's maximum gain with the transmission coefficient, τ , at 865 MHz was $G_{max}^{tag} \tau = -0.5$ dB [34]. Since we could not measure each component's field separately and the direction of arrival of the measured field was not necessarily at the direction of maximum gain of the tag's antenna, we considered 1.5 dB additional losses due to the radiation pattern of the tag's antenna. Hence, we assumed $G_{max}^{tag} \tau = -2$ dB. The corresponding power, P_{thres} , at the location of the tag was then -16 dBm:

$$P_{thres}[\text{dBm}] = P_{thres}^{IC}[\text{dBm}] - G^{tag} \tau[\text{dB}]. \quad (17)$$

Finally, the measured received power at the location of the i th tag, P_{inc}^i , corresponding to a reader transmission power level $T_{max} = 30$ dBm, was

$$P_{inc}^i = P_{thres} + (T_{max} - T_i^{min}). \quad (18)$$

For example, for $T_i^{min} = 18$ dBm, we had $P_{inc}^i = -16$ dBm + (30 dBm - 18 dBm) = -4 dBm.

The proposed method allowed us to map the measured received power within a dynamic range of 15 dB, limited only by the available minimum and maximum transmission-power settings of the reader. By measuring the field in the entire volume of interest, we could identify maxima and minima inside the room, as demonstrated in the characteristic results of Figures 18 and 19. In these figures, the MT-242032/NRH 7 dBiC antenna was connected to the reader in Measurements Configuration II. Figure 18 shows the measured received power as calculated by Equation (18) for the vertically polarized tags, and Figure 19 shows the measured field for the horizontally polarized tags. The locations of two important scatterers are also mapped in these figures.

7.2 Coverage Results

For each power-transmission level, we measured the number of identified tags per polarization axis, and divided it into the corresponding total number of same-polarization tags. Also, in order to evaluate tag diversity, for each transmission power level, we measured the tags' diversity identification percentage by considering each position as identified if either the vertically or the horizontally polarized tag at that position was identified. The corresponding coverage plot for the Measurements Configuration II for both polarizations and tag diversity is given in Figure 20. Coverage improvement, on the order of 10% for transmitted power smaller than 24 dBm, was recorded by implementing tag diversity.

7.3 Performance Evaluation

7.3.1 Single-Antenna Configurations

The identification performance of the single-antenna Measurements Configurations I and II, assuming tag diversity, is shown in Figure 21. Better performance was recorded in both configurations when the 10 dBiC antenna was connected to the reader, benefiting from the increased gain combined with the reduced dimensions of the measurement volume: width \times length \times height = 2.5 m \times 2 m \times 0.5 m. As a result, the narrow beamwidth of the 10 dBiC antenna was sufficient for the correspondingly narrower measurement volume with respect to the actual wall-to-wall dimensions of the room.

7.3.2 Double-Antenna Configurations

As discussed earlier, the double-antenna configurations were measured with and without the delay line of Figure 17. The

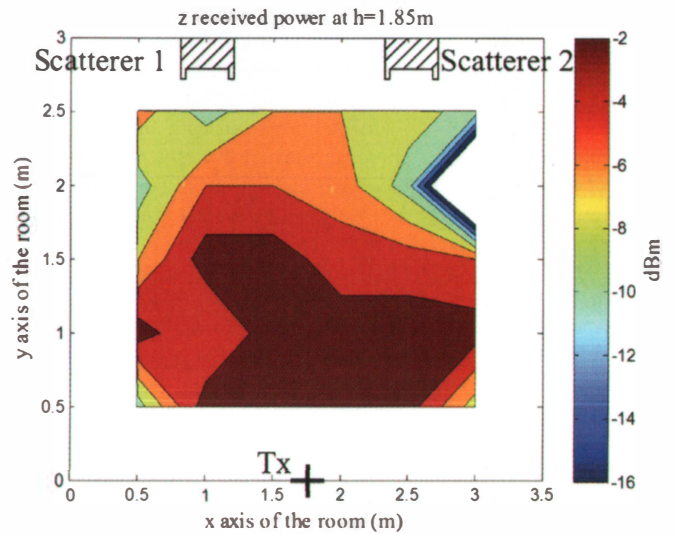


Figure 18. The z-polarized measured power.

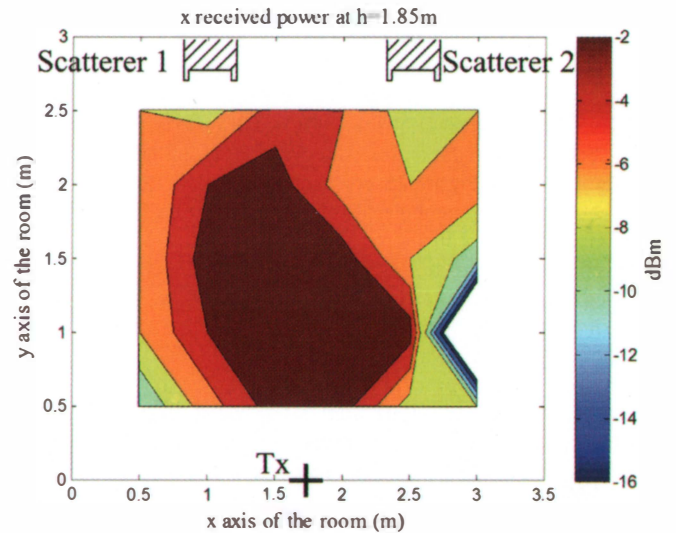


Figure 19. The x-polarized measured power.

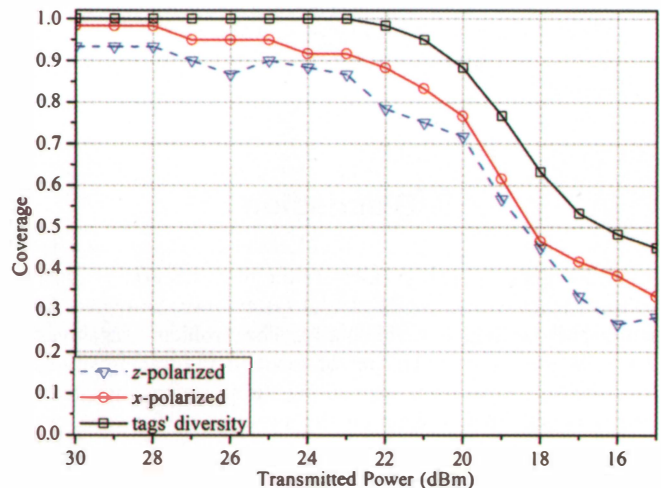


Figure 20. The coverage performance for Measurement Configuration II.

resulting field patterns inside the room were notably different in the two measurement states, verifying the theoretical benefits of the introduction of the proposed phase shifter. Two characteristic results are shown in Figures 22 and 23, corresponding to Measurements Configuration IV (7 dBic antennas), with and without the delay line, respectively. The locations of the antennas are also drawn. Two important remarks are appropriate in connection with these figures. First, when the two antennas radiated with no phase difference, a minimum was recorded centrally in the room (Figure 22), due to destructive interference of the direct field of the two antennas, which vanishes upon insertion of the delay line (Figure 23). Second, a second minimum is shown in Figure 22, in the vicinity of a strong scatterer at the top-left area of the room. This minimum could not be shifted by inserting the phase delay (Figure 23), because it resulted from the interaction of the transmitted field with the environment; hence, all related contributions were equally delayed.

A representative result, demonstrating the identification performance gain by implementing the proposed phase shifter, is shown in Figure 24 for Measurements Configuration III for the 7 dBic antennas. In Figure 25, the combined (with and without the delay line) performance of all double-antenna configurations with both antenna types is presented. The corresponding coverage results for the best single-antenna configuration are also given as a reference. In order to carry out a fair comparison, we assigned 4 dB losses in the single-antenna case, equal to the insertion losses of the available splitter (not the 3 dB splitting loss per antenna). Hence, the 30 dBm transmission power level of Measurements Configuration II in Figure 25 corresponded to the 26 dBm measured identification percentage of the same configuration, shown in Figure 21. This was considered “fair” as the insertion losses of a quality commercial splitter are of the order of 0.1 dB [35]. Three double-antenna configurations were comparable to, and in some cases, slightly better than, the best single-antenna configuration. Measurements Configuration V was expected to have slightly worse performance. The main reason was that due to the horizontal and vertical tilting, a significant y -polarized component was transmitted, which was not received by any tag (only x and z polarization were measured). This fact also explains why Configuration III demonstrated the best performance, since all the transmitted energy of the circularly polarized antenna was distributed in the x - and z -polarization axes.

Finally, in Figure 26, we measured the performance of the scheme proposed in Section 6.2, where each of the antennas in the double-antenna configurations transmitted in a unique timeslot. The best single-antenna performance is given as a reference. As expected, good performance was experienced, for the reasons discussed earlier.

8. Discussion

In this paper, planning rules for the identification of passive tags inside a room from a UHF RFID system were extracted theoretically and verified experimentally. The problem was investigated in for the three dimensions of space. A ray-tracing site-specific model was developed, accounting for all propagation factors of the problem. Their effects on the system’s performance were thoroughly analyzed.

Multipath creates constructive and destructive interference patterns inside a room. It was shown that the coverage performance inside a room with no other obstacles could be better than the

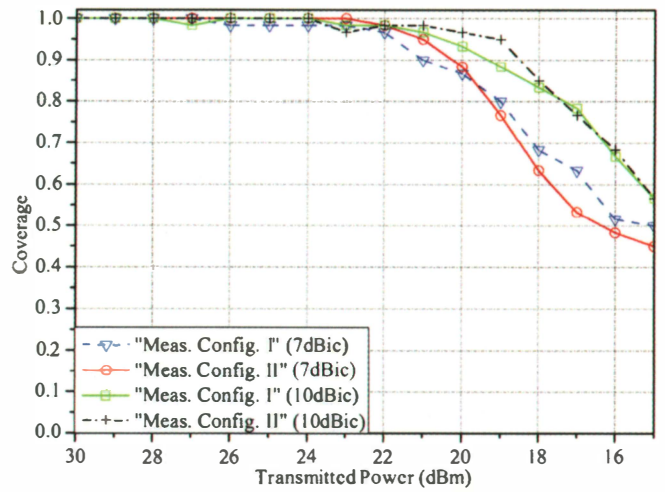


Figure 21. The coverage performance of the four single-antenna configurations.

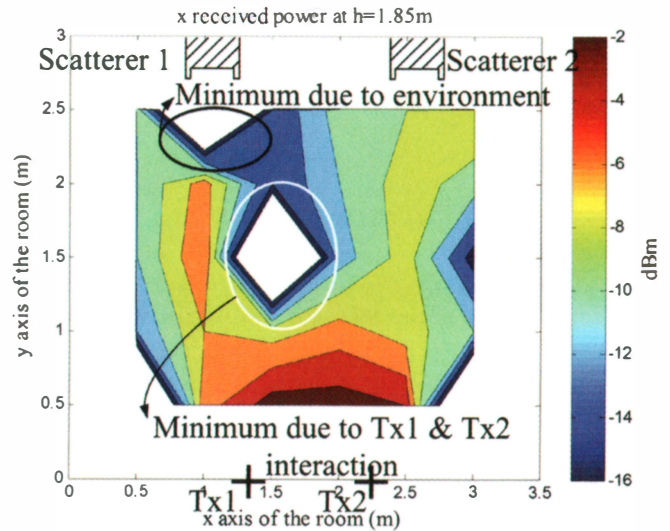


Figure 22. The x -polarized measured power for Configuration IV without a delay line.

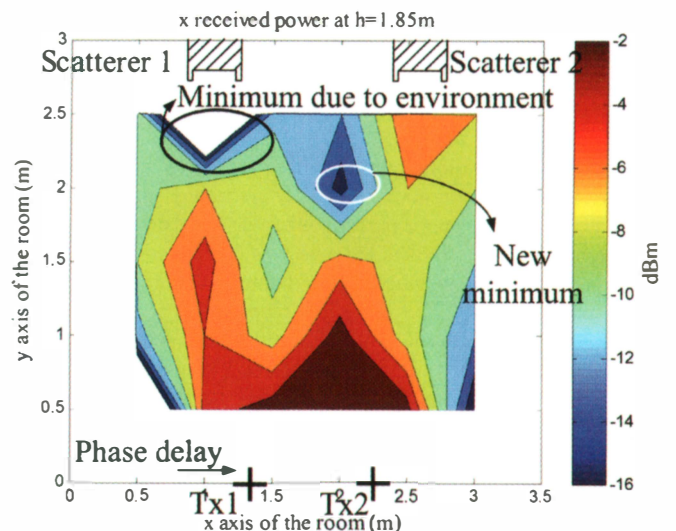


Figure 23. The x -polarized measured power for Configuration IV with a delay line.

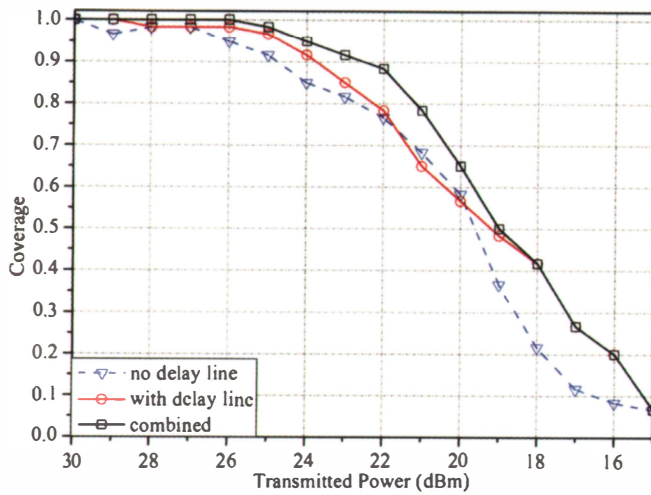


Figure 24. The performance gain by implementing the proposed phase shifter for Measurement Configuration III.

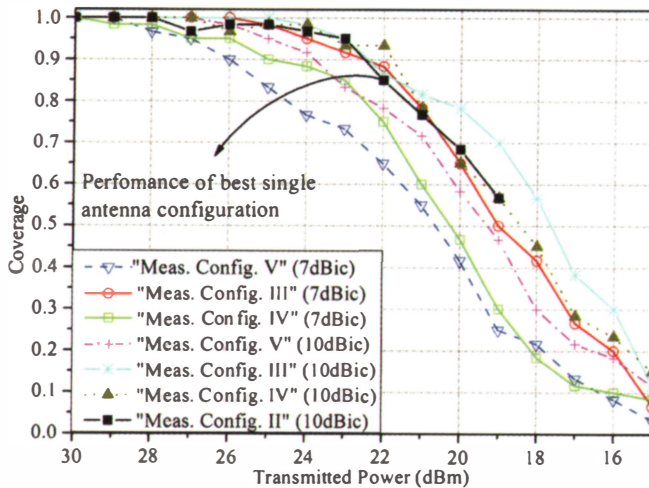


Figure 25. The performance of all double-antenna configurations by implementing the proposed phase shifter.

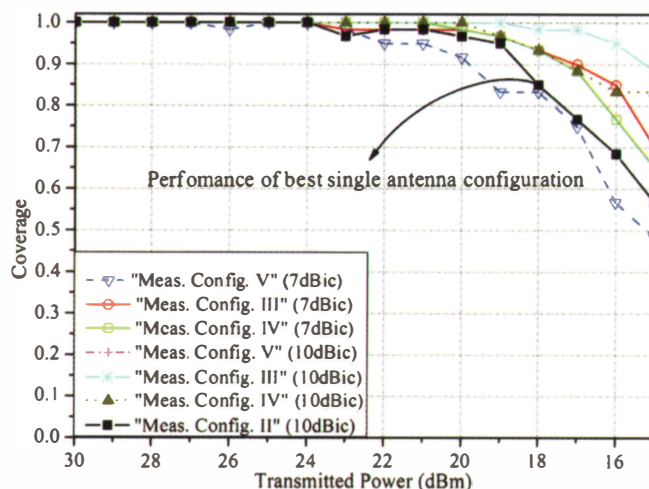


Figure 26. The performance of all double-antenna configurations by implementing the proposed alternating-transmission scheme.

performance exhibited in free-space conditions in the same volume as the one limited by the room's walls, depending on the size of the volume. This was due to the entrapment of a greater part of the radiated field inside the room. However, the reliability of "coverage" at a given point in "real conditions" was challenged: "holes" of coverage were introduced in the volume of interest.

In single-antenna configurations, "holes" existed due to the interaction of the transmitted field with the environment. They were typically expected in the vicinity of the walls or other scatterers located in the room, because in these regions, the magnitude of the scattered field was comparable to that of the direct field.

In multiple-antenna configurations, "holes" were also formed due to the interaction of the transmitted fields from the two antennas. This property can be exploited advantageously, if minima of the field are desired in specific locations inside a room (e.g., the sensitive volume, where a patient lies above the bed).

If coverage maximization is sought, a single-antenna configuration should be preferred, in order to avoid the additional-destructive interference patterns. However, when the radiation pattern of a single antenna is inadequate, then multiple-antenna configurations can be exploited. In such a case, several methods were put forward to minimize "coverage holes" in the volume of interest. One was to place the antennas in such manner that minimum interaction among them is maintained in the volume of interest. As a simple rule, the 3 dB angular volumes of the radiation patterns of the antennas should not cross. A better idea is to implement the proposed switch-controlled phase shifter in the feeding path of one of the antennas. In the two states of the switch, the minima, due to the direct field of the antennas, are shifted. In such a case, interaction between the antennas acts beneficially for the performance of the system, and should be sought in the planning process. A last method is to schedule the transmission of each of the antennas, allowing only one antenna to operate at each time. The benefit of this technique is the avoidance of the 3 dB splitting coupling per antenna, and the avoidance of the destructive interference patterns due to the antennas' interaction. The proposed methods can be combined with others, as in [4], discussed earlier, or in [37], where power-optimized waveforms, suitable for operation of the charge-pump of a passive tag, were shown, and greatly improved the identification performance of future RFID systems.

Finally, tags' polarization-diversity gains of the order of 10% were found. Such a scheme could be implemented when the dimensions of the target object allow.

9. References

1. D. M. Dobkin, *The RF in RFID: Passive UHF RFID in Practice*, Oxford, Boston, Newnes (Elsevier), 2008.
2. J. D. Griffin and G. D. Durgin, "Complete Link Budgets for Backscatter-Radio and RFID Systems," *IEEE Antennas and Propagation Magazine*, **51**, 2, April 2009, pp. 11-25.
3. A. Lázaro., D. Girbau, and D. Salinas, "Radio Link Budgets for UHF RFID on Multipath Environments," *IEEE Transactions on Antennas and Propagation*, **AP-57**, 4, April 2009, pp. 1241-1251.
4. J. D. Griffin and G. D. Durgin, "Gains For RF Tags Using Multiple Antennas," *IEEE Transactions on Antennas and Propagation*, **AP-56**, 2, February 2008, pp. 563-570.

5. G. Marrocco, E. Di Giampaolo, and R. Aliberti, "Estimation of UHF RFID Reading Regions in Real Environments," *IEEE Antennas and Propagation Magazine*, **51**, 6, December 2009, pp. 44-57.
6. A. C. Polycarpou, G. Gregoriou, A. Bletsas, A. Dimitriou, J. Sahalos, "A UHF Radio Frequency Identification (RFID) System for Healthcare: Design and Implementation," International ICST Conference on Wireless Mobile Communication and Healthcare (2010 MOBIHEALTH), Ayia Napa, Cyprus, October 2010.
7. A. G. Dimitriou, A. Bletsas, A. Polycarpou, and J. N. Sahalos, "Coverage Improvement of an RFID System inside a Room," COST ic0603 (Antennas Systems & Sensors for Information Society Technologies), Wroclaw, October 2009.
8. A. G. Dimitriou, A. Bletsas, and J. N. Sahalos, "On Efficient UHF RFID Coverage inside a Room," European Conference on Antennas and Propagation (EuCAP 2010), Barcelona, April 2010.
9. S. R. Saunders, *Antennas and Propagation for Wireless Communication Systems*, New York, John Wiley & Sons, 1999.
10. A. G. Dimitriou, *Estimation and Experimental Validation of the Transmission of Electromagnetic Waves in Urban Environment*, PhD dissertation, 2006.
11. M. F. Catedra and J. Perez-Arriaga, *Cell Planning for Wireless Communications*, Norwood, MA, Artech House, 1999.
12. C. A. Balanis, *Advanced Engineering Electromagnetics*, New Jersey, John Wiley & Sons, 1989.
13. J. B. Hasted and M. A. Shah. "Microwave Absorption by Water in Building Materials," *British Journal of Applied Physics*, **15**, 1964, pp. 825-836.
14. O. Landron, M. J. Feuerstein, and T. S. Rappaport, "A Comparison of Theoretical and Empirical Reflection Coefficients for Typical Exterior Wall Surfaces in a Mobile Radio Environment," *IEEE Transactions on Antennas and Propagation*, **AP-44**, 3, March 1996, pp. 341-351.
15. R. Peña, R. Feick, H. D. Hristov, and W. Grote, "Measurement and Modeling of Propagation Losses in Brick and Concrete Walls for the 900-MHz Band," *IEEE Transactions on Antennas and Propagation*, **AP-51**, 1, January 2003, pp. 31-39.
16. C. Oestges, B. Clerckx, L. Raynaud, and D. Vanhoenacker-Janvier, "Deterministic Channel Modeling and Performance Simulation of Microcellular Wide-Band Communication Systems," *IEEE Transactions on Vehicular Technology*, **51**, 6, November 2002, pp. 1422-1430.
17. A. Bletsas, A. G. Dimitriou, and J. N. Sahalos, "Improving Backscatter Radio Tag Efficiency," *IEEE Transactions on Microwave Theory and Techniques*, **58**, 6, May 2010, pp. 1502-1509.
18. C. A. Balanis, *Antenna Theory: Analysis and Design, Third Edition*, New York, John Wiley and Sons, 2005.
19. P. V. Nikitin, K. V. S. Rao, R. Martinez, and S. F. Lam, "Sensitivity and Impedance Measurements of UHF RFID Chips," *IEEE Transactions on Microwave Theory and Techniques*, **57**, 5, part 2, May 2009, pp. 1297-1302.
20. "UHF Gen 2 RFID Speedway Reader (IPJ-R1000), Octane 3.0 User Guide", Impinj, Seattle, Washington USA.
21. "UCODE G2XM and UCODE G2XL Data Sheet," NXP, Eindhoven, The Netherlands.
22. "IPJ-P5002-D2 Data Sheet," Impinj, Seattle, Washington USA.
23. "Higgs-3 Data Sheet," Alien, Morgan Hill, California, USA.
24. J. D. Griffin, G. D. Durgin, A. Haldi, and B. Kippelen, "RF Tag Antenna Performance on Various Materials Using Radio Link Budgets," *IEEE Antennas and Wireless Propagation Letters*, **5**, 1, 2006, pp. 247-250.
25. "MT-242017/NRH Data Sheet," "MT-242032/NRH Data Sheet," MTI Wireless Edge Ltd., Israel.
26. A. Papoulis and S. U. Pillai, *Probability, Random Variables and Stochastic Processes, Fourth Edition*, New York, McGraw Hill, 2002.
27. N. C. Karmakar, S. M. Roy, and M. S. Ikram, "Development of Smart Antenna for RFID Reader," IEEE International Conference on RFID, 2008, pp. 65-73.
28. J.-D. Tseng, R.-J. Ko, and W.-D. Wang, "Switched Beam Antenna Array for UHF Band RFID System," IEEE International Workshop on Anti-Counterfeiting, Security, Identification, 2007, pp. 92-95.
29. M. Abbak, I. Tekin, "RFID Coverage Extension Using Microstrip-Patch Antenna Array," *IEEE Antennas and Propagation Magazine*, **51**, 1, February 2009, pp. 185-191.
30. P. Salonen and L. Sydanheimo, "A 2.45 GHz Digital Beam-Forming Antenna for RFID Reader," IEEE 55th Vehicular Technology Conference, **4**, Spring 2002, pp. 1766-1770.
31. J. D. Griffin and G. D. Durgin, "Multipath Fading Measurements for Multi-Antenna Backscatter RFID at 5.8 GHz," IEEE International Conference on RFID, 2009, pp. 322-329.
32. J. D. Griffin and G. D. Durgin, "Multipath Fading Measurements at 5.8 GHz for Backscatter Tags with Multiple Antennas," *IEEE Transactions on Antennas and Propagation*, **AP-58**, 11, November 2010, pp. 3693-3700.
33. S. Capdevila, L. Jofre, J. Romeu, and J. Ch. Bolomey, "RFID Array Sensing," European Conference on Antennas and Propagation (EuCAP 2010), Barcelona, April 2010.
34. "ALN-9662 Squiggle-SH Inlay Data Sheet," Alien, Morgan Hill, California, USA.
35. "PD1020 – Two-Way Power Divider, 0.7-2.7 GHz, 40 Watts Data Sheet," INSTOCK Wireless Components Inc, New Jersey, USA.
36. J.-P. Curty, M. Declercq, C. Dehollain, and N. Joehl, *Design and Optimization of Passive UHF RFID Systems*, New York, Springer, 2007.
37. M. S. Trotter, J. D. Griffin, and G. D. Durgin, "Power-Optimized Waveforms for Improving the Range and Reliability of RFID Systems," IEEE International Conference on RFID, 2009, pp. 80-87.

Introducing the Authors



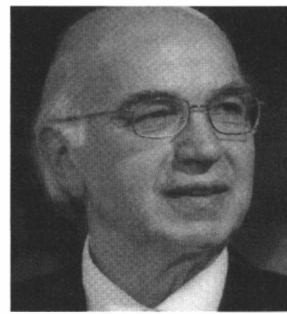
Antonis G. Dimitriou received the diploma and the PhD degree in Electrical and Computer Engineering from the Aristotle University of Thessaloniki (AUTH), Greece, in 2001, and 2006, respectively. Since 2007, he has been with the Department of Electrical and Computer Engineering of AUTH.

Since 2001, he has participated in 16 research projects in the fields of communications, antennas, propagation, signal processing, and RFIDs, including the design of a DCS-1800 cellular network that operated within the Olympic stadium during the 2004 Olympic Games, and a pilot implementation of an RFID system in a hospital in Nicosia. He is the author or coauthor of approximately 30 journal and conference papers. His current interests are in the areas of electromagnetic-wave propagation, planning and optimization of wireless networks, relay techniques in wireless communications and RFIDs. Dr. Dimitriou was the recipient of the Ericsson Award of Excellence in Telecommunications for the best undergraduate thesis in 2001.



Aggelos Bletsas received with excellence his diploma degree in Electrical and Computer Engineering from Aristotle University of Thessaloniki, Greece in 1998, and the SM and PhD degrees from Massachusetts Institute of Technology in 2001 and 2005, respectively. He worked at Mitsubishi Electric Research Laboratories (MERL), Cambridge, MA, as a Postdoctoral Fellow, and at the Radiocommunications Laboratory (RCL), Department of Physics, Aristotle University of Thessaloniki, as a visiting scientist. He joined the Electronic and Computer Engineering Department, Technical University of Crete, in summer of 2009, as an Assistant Professor.

His research interests focus on scalable wireless communication and networking, with emphasis on relay techniques, signal processing for communication, radio hardware/software implementations for wireless transceivers and low-cost backscatter sensor networks, RFID, time/frequency metrology, and bibliometrics. Dr. Bletsas was the co-recipient of the IEEE Communications Society 2008 Marconi Prize Paper Award, and the best paper distinction at IEEE ISWCS 2009, Siena, Italy.



John N. Sahalos received his BSc in Physics in 1967, and his PhD in Physics in 1974, from the Aristotle University of Thessaloniki, (AUTH), Greece. Except of his PhD, during 1970-75, he studied at the School of Engineering of AUTH and he received the Diploma (BCE+MCE) in Civil Engineering in 1975. During 1972-1974, he also studied at the School of Science of AUTH, and he received the professional Diploma of postgraduate studies in Radio-Electrology in 1975.

From 1971 to 1974, he was a Teaching Assistant at the Department of Physics, AUTH, and from 1974 to 1976 he was an Instructor there. In 1976, he worked at the ElectroScience Laboratory, the Ohio State University, Columbus, as a Postdoctoral University Fellow. From 1977 to 1986, he was a Professor in the Electrical Engineering Department, University of Thrace, Greece, and Director of the Microwaves Laboratory. From 1986 to 2010, he was a Professor at the School of Science, AUTH, where he was the director of the postgraduate studies in Electronic Physics and the director of the Radio-Communications Laboratory (RCL). Dr. Sahalos is now Professor in the Electrical and Computer Engineering Department of the University of Nicosia, Cyprus, and Director of the Radio & Telecommunications Laboratory (RTeLab).

During 1981-82, he was a visiting Professor at the Department of Electrical and Computer Engineering, University of Colorado, Boulder. During 1989-90, he was a visiting Professor at the Technical University of Madrid, Spain. He is the author of three books in Greek, of seven book chapters, and more than 350 articles published in the scientific literature. He also is the author of the book *The Orthogonal Methods of Array Synthesis, Theory and the ORAMA Computer Tool* (Wiley, 2006). His research interests are in the areas of antennas, high-frequency techniques, communications, EMC/EMI, microwaves, and biomedical engineering. Dr. Sahalos is a Professional Engineer and a consultant to industry. In 2002-2004, he was on the Board of Directors of the OTE, the largest Telecommunications Company in southeast Europe. He served as a technical advisor in several national and international committees, as well as in several mobile communications companies. Since 1992, he has been a member of Commissions A and E of the Greek National Committee of URSI. Since 1998, he has been the President of the Greek committee of URSI. He was the President of the Section of Informatics, Telecommunications and Systems of the National Committee of Research and Technology. Dr. Sahalos is a Life Fellow of the IEEE. He also is a member of the Greek Physical Society, an Honor Fellow of Radio-Electrology and a member of the Technical Chamber of Greece. He is the creator and leader of an EMC network with five laboratories (three from academia and two from industry). He has been honored with a special investigation fellowship of the Ministry of Education & Science, Spain. He also has been honored by several institutes and organizations. He has been on the editorial board of three scientific journals. Dr. Sahalos was elected by the department representatives of the Aristotle University of Thessaloniki as the Vice Chairman of the Research Committee of AUTH for the period 2007-2010. Since 2010, he has been a member of the University of Nicosia Research

Foundation (UNRF), and a member of the consulting committee of the GRNET SA. He has supervised 25 PhDs and more than 100 postgraduate-diploma theses. With his colleagues, Prof. Sahalos designed several well-known innovative products such as electric impedance tomography, (EIT), microwave landing system (MLS), the ORAMA simulator, and the SMS-K monitoring system. (16)